Characterization and genomic analysis of the Lyme disease spirochete bacteriophage ϕBB-1

Dominick R. Faith[1]*, Margie Kinnersley[1]*, Diane M. Brooks[1], Dan Drecktrah[1], Laura S. Hall[1], Eric Luo[2], Andrew Santiago-Frangos[3], Jenny Wachter[2], D. Scott Samuels[1], and Patrick R. Secor[1#]

[1] Division of Biological Sciences, University of Montana, Missoula, MT, USA

[2] Vaccine and Infectious Disease Organization, Saskatoon, SK, Canada

[3] Department of Biology, University of Pennsylvania, Philadelphia, PA, USA

*These authors contributed equally to this work

[#] Correspondence: Patrick.secor@mso.umt.edu

Abstract

Lyme disease is a tick-borne infection caused by the spirochete *Borrelia* (*Borreliella*) *burgdorferi*. *Borrelia* species have highly fragmented genomes composed of a linear chromosome and a constellation of linear and circular plasmids some of which are required throughout the enzootic cycle. Included in this plasmid repertoire by almost all Lyme disease spirochetes are the 32-kb circular plasmid cp32 prophages that are capable of lytic replication to produce infectious virions called ϕBB-1. While the *B. burgdorferi* genome contains evidence of horizontal transfer, the mechanisms of gene transfer between strains remain unclear. While we know that ϕBB-1 transduces cp32 and shuttle vector DNA during *in vitro* cultivation, the extent of ϕBB-1 DNA transfer is not clear. Herein, we use proteomics and long-read sequencing to further characterize ϕBB-1 virions. Our studies identified the cp32 *pac* region and revealed that ϕBB-1 packages linear cp32s via a headful mechanism with preferentially packaging of plasmids containing the cp32 *pac* region. Additionally, we find ϕBB-1 packages fragments of the linear chromosome and full-length plasmids including lp54, cp26, and others. Furthermore, sequencing of ϕBB-1 packaged DNA allowed us to resolve the covalently closed hairpin telomeres for the linear *B. burgdorferi* chromosome and most linear plasmids in strain CA-11.2A. Collectively, our results shed light on the biology of the ubiquitous ϕBB-1 phage and further implicates ϕBB-1 in the generalized transduction of diverse genes and the maintenance of genetic diversity in Lyme disease spirochetes.

Introduction

The bacterium *Borrelia* (*Borreliella*) *burgdorferi* is the causative agent of Lyme disease, the most common tick-borne disease in the Northern Hemisphere [1-3]. Lyme disease spirochetes have complex and highly fragmented genomes composed of a ~900-kb linear chromosome and up to twenty distinct and co-existing linear and circular plasmids that are similar but not identical across the genospecies [4-6].

As a vector-borne pathogen, *B. burgdorferi* relies on the differential expression of several outer surface lipoproteins to transmit from its tick vector to a vertebrate host [7]. As such, a large fraction of the *B. burgdorferi* genome encodes outer membrane lipoproteins, mostly carried on the plasmids [6, 8, 9].

In natural populations, genetic variation in outer membrane lipoprotein alleles is associated with species-level adaptations [6, 8-10] and variation in outer membrane lipoprotein alleles across the genospecies is driven primarily by horizontal gene transfer [5, 11-21]. However, the mechanism(s) by which heterologous *B. burgdorferi* strains exchange genetic material are not well defined.

Viruses that infect bacteria (phages) are key drivers of horizontal gene transfer between bacteria [22]. The genomes of nearly all sequenced Lyme disease spirochetes include the 32-kb circular plasmid (cp32) prophages (**Fig 1A and B**) [4]. The cp32s carry several outer membrane lipoprotein gene families including *bdr, mlp*, and *ospE/ospF/elp* (*erps*), which are all involved in immune evasion [23-27] and exhibit sequence variation that is consistent with historical recombination amongst cp32 plasmid isoforms [21, 28, 29]. Recent work indicates that cp32 prophages are induced in the tick midgut during a bloodmeal [9, 30, 31]. When induced, cp32 prophages undergo lytic replication where they are packaged into infectious virions designated ϕBB-1 (**Fig 1C**) [32-34].

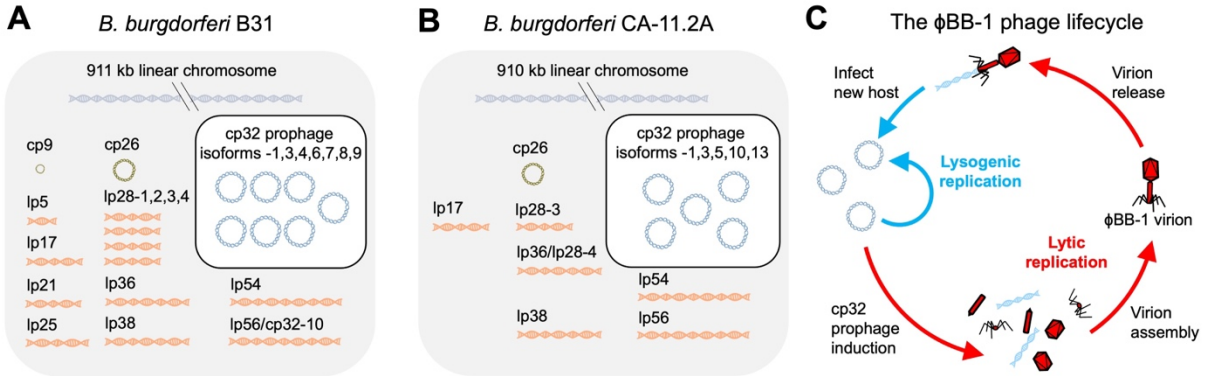

Figure 1. The *B. burgdorferi* genome is highly fragmented and is composed of a linear chromosome, linear and circular plasmids, and cp32 prophages. The genomes of *B. burgdorferi* strains **(A)** B31 and **(B)** CA-11.2A are shown. **(C)** The temperate ϕBB-1 phage lifecycle is depicted.

In addition to horizontally transferring phage genomes between bacterial hosts (transduction), phages frequently package and horizontally transfer pieces of the bacterial chromosome or other non-phage DNA (generalized transduction) [35]. Generalized transduction was first observed in the *Salmonella* phage P22 in the 1950s [36] and since then has been observed in numerous other phage species [35, 37-40]. ϕBB-1 is a

generalized transducing phage that can horizontally transfer shuttle vectors carrying antibiotic resistance cassettes between *B. burgdorferi* strains [32]. However, to our knowledge, generalized transduction of anything other than engineered plasmids by ϕBB-1 has not been observed.

Here, we define the genetic material packaged by ϕBB-1 virions isolated from *B. burgdorferi* strain CA-11.2A. Our proteomics studies confirm that ϕBB-1 virions are composed primarily of capsid and other phage structural proteins encoded by the cp32s; however, putative phage structural proteins encoded by lp54 were also detected. Long-read sequencing reveals that ϕBB-1 virions package a variety of genetic material including cp32 isoforms that are linearized at a region immediately upstream of the *erp* locus (*ospE/ospF/elp*) and packaged into ϕBB-1 capsids via a headful genome packaging mechanism at a packaging site (*pac*). When introduced to a shuttle vector, the *pac* region promotes the packaging of shuttle vectors into ϕBB-1 virions, demonstrating the utility of ϕBB-1 as a tool to genetically manipulate Lyme disease spirochetes. Additionally, full-length contigs of cp26, lp17, lp38, lp54, and lp56 are recovered from packaged reads as are fragments of the linear chromosome. Finally, long-read sequencing of packaged DNA allowed us to fully resolve most of the covalently closed hairpin telomeres in the *B. burgdorferi* CA-11.2A genome.

Overall, this study implicates ϕBB-1 in mobilizing large portions of the *B. burgdorferi* genome, which may explain certain aspects of genome stability and diversity observed in Lyme disease spirochetes.

Results

ϕBB-1 phage purification, virion morphology, and proteomic analysis

In the laboratory, lytic ϕBB-1 replication (**Fig 1C**) can be induced by fermentation products such as ethanol [41, 42]. We first measured ϕBB-1 titers in early stationary-phase cultures (~1 × 10^8 cells/mL) of *B. burgdorferi* B31 or CA-11.2A induced with 5% ethanol, as described by Eggers *et al.* [41]. Seventy-two hours after induction, bacteria were removed by centrifugation and filtering. Virions were then purified from supernatants by chloroform extraction and precipitation with ammonium sulfate. Purified virions were treated for one hour with DNase to destroy DNA not protected within a capsid and re-chloroformed to inactivate DNAse and quantitative PCR (qPCR) was used to measure packaged cp32 copy numbers.

B. burgdorferi strain CA-11.2A consistently produced ~10 times more phage than B31 (**Fig 2A**) and was selected for further study. Imaging of purified virions collected from CA-11.2A by transmission electron microscopy reveals virions with an elongated capsid and contractile tail (**Fig 2B**), which is similar to the Myoviridae morphology of ϕBB-1 virions produced by strain B31 *in vitro* [9, 43, 44] and by a human *B. burgdorferi* isolate following ciprofloxacin treatment [45].

Mass spectrometry analysis of purified virions identified ten capsid and other structural proteins encoded by the cp32s including the major capsid protein and capsid fibers (**Fig 2C, Table S1**). We also detected highly conserved predicted phage capsid

proteins encoded by lp54 (**Fig 2D**). While the virions we visualized all appear to have the same elongated capsid morphology, virions with a notably smaller capsid morphology have been isolated and imaged from *B. burgdorferi* CA-11.2A [32]. These observations raise the possibility that there are multiple intact phages inhabiting the CA-11.2A genome.

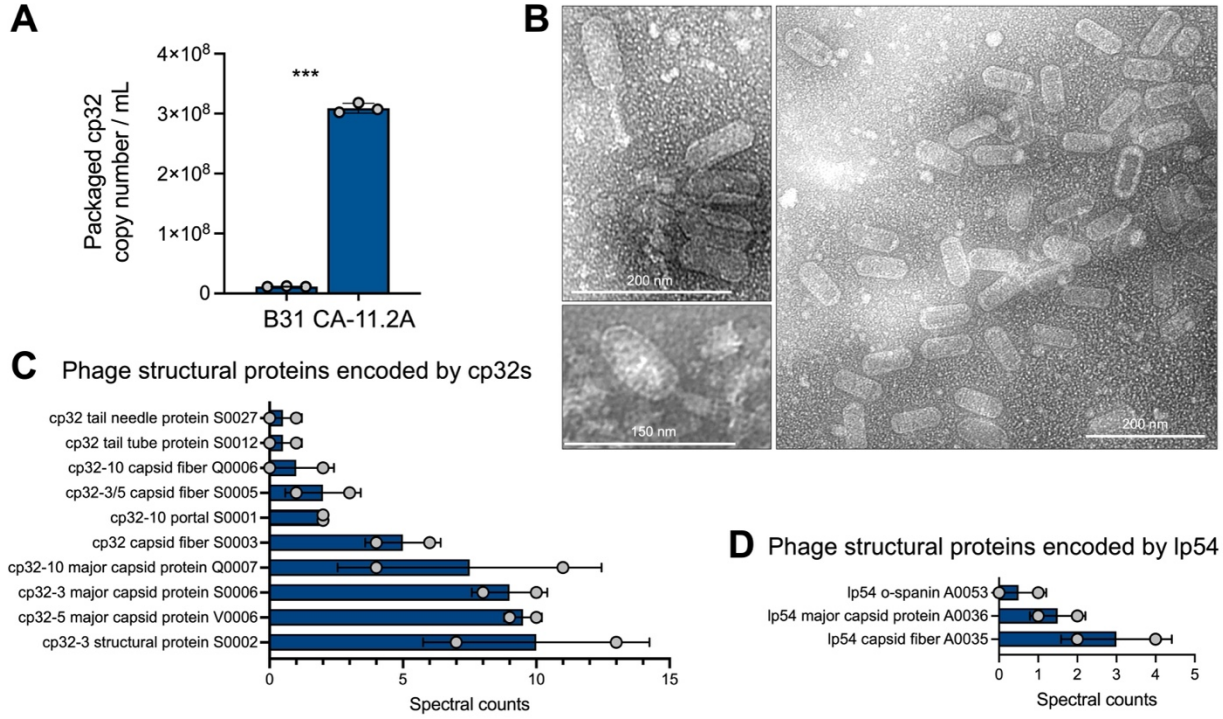

Figure 2. ϕBB-1 phage titer, virion morphology, and proteomic analysis. (A) Packaged, DNase-protected cp32 copy numbers in bacterial supernatants were measured by qPCR. Data are the SE of the mean of three experiments, ***p <0.001. **(B)** Virions were purified from 4-L cultures of *B. burgdorferi* CA-11.2A and imaged by transmission electron microscopy. Representative images from two independent preparations are shown. **(C and D)** HPLC-MS/MS-based proteomics was used to identify proteins in two purified virion preparations. The SE of the mean of spectral counts for peptides associated with the indicated phage structural proteins are shown for each replicate. See also **Table S1** for the complete proteomics dataset.

ϕBB-1 virions package portions of the *B. burgdorferi* genome

We performed long-read sequencing on DNA packaged in purified ϕBB-1 virions, as outlined in **Figure 3**. Although intact *B. burgdorferi* cells were removed via both centrifugation and filtration prior to chloroform treatment, there is concern that contaminating unpackaged *B. burgdorferi* chromosomal or plasmid DNA co-purifies with phage virions. To control for this, we spiked purified ϕBB-1 virions with high molecular weight (>20 kb) salmon sperm DNA (**Fig 4A**) at 1.7 µg/mL, a concentration that approximates the amount of DNA released by 3 × 10^8 lysed bacterial cells into one milliliter of media [46]. Samples were then treated with DNase overnight followed by phage DNA extraction using a proteinase K/SDS/phenol-chloroform DNA extraction protocol [33]. Purified DNA was directly sequenced using the Nanopore MinION (long read) platform.

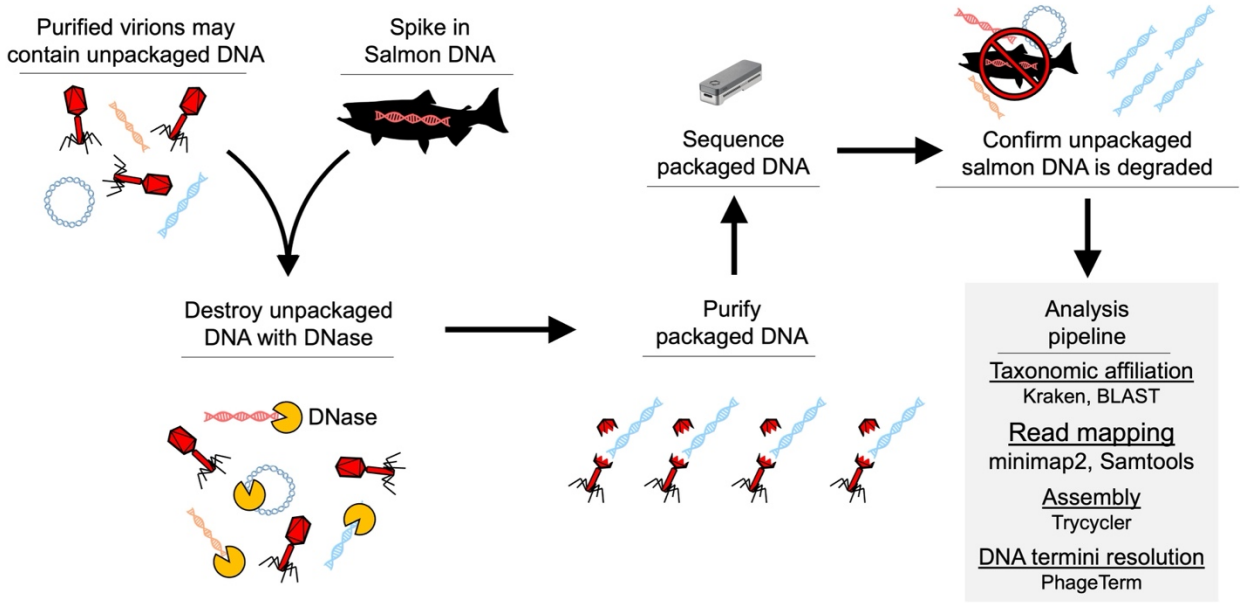

Figure 3. Workflow for sequencing packaged ϕBB-1 DNA.

Across three replicates, we recovered a total of 110,986 nanopore reads >700 bp in length that met a minimum q-score threshold of 7. Kraken [47] and BLAST analyses indicated that the DNase treatment successfully degraded unpackaged DNA, as only 155 reads (0.14% of the total) with an average length of 1.2kb were derived from the salmon-sperm DNA spike-in (**Fig 4B**). To further reduce the possibility of unpackaged *B. burgdorferi* DNA carryover, we imposed a stringent 5kb read-length cutoff, thus reducing the number of salmon-derived reads to zero and leaving a total of 58,399 reads (**Fig 4C**) with a median length of ~12.3 kb (**Fig 4D**). Note that we detected a high number of ~32 kb reads in each replicate which are the approximate size of cp32 prophages (**Fig 4D**, dashed line).

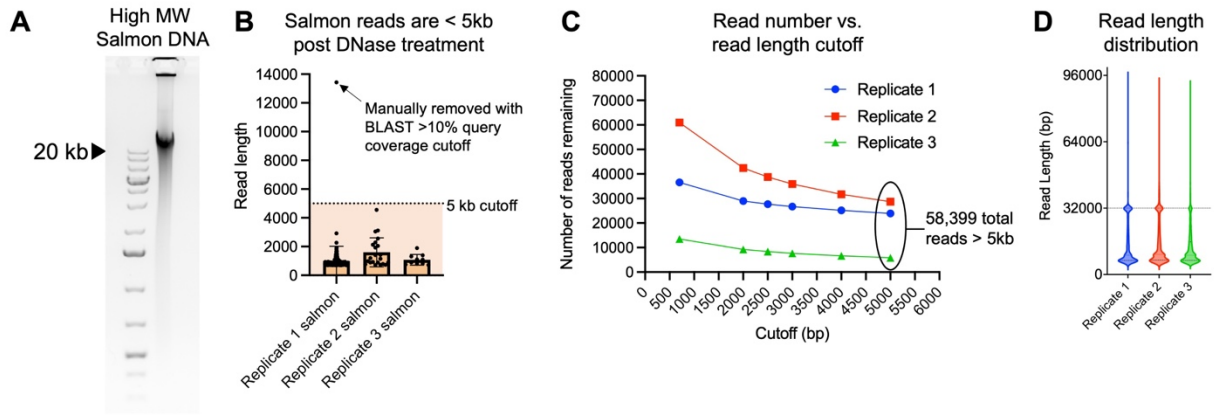

Figure 4. Establishing a 5kb read length cutoff to exclude unpackaged reads. (A) The salmon sperm DNA used to spike purified phages prior to DNase treatment was run on an agarose gel to estimate its size. Note that the majority of salmon DNA is larger than the 20-kb high molecular weight marker in the left lane. **(B)** 0.14% of 110,986 reads > 700 bp, 0.14% were classified as matching salmon sequences. Reads classified as salmon were plotted as a function of their length for each replicate. Error bars represent the SE of the mean of three replicate experiments. All reads except one (arrow) were below 5 kb in length (dashed line) with an average length of 1.2 kb. **(C)** Read length cutoff was plotted as a function of the

number of reads remaining in each replicate dataset. In total, 58,399 reads remain after establishing a 5-kb cutoff. **(D)** Read length for all reads >5 kb in each replicate was plotted.

Overall, ~99.6% of packaged reads >5 kb were classified as *B. burgdorferi* (**Fig 5A**), the majority of which (~79%) were cp32 isoforms (**Fig 5B**). Cp32-10 and cp32-3 were preferentially packaged (~32% and ~25%, respectively) followed by cp32-13 and cp32-5 (each at ~10%) (**Fig 5B**). Reads mapping to cp32-3, cp32-5, cp32-10, and cp32-13 had a mean coverage of over 1,000× (**Fig 5C**). Cp32-1 reads accounted for only about one percent of all packaged reads (**Fig 5B**) and had lower mean coverage of approximately 36× (**Fig 5C**), suggesting that cp32-1 was not undergoing lytic replication. Read length distributions across cp32s indicate that full-length ~32 kb molecules were often recovered for cp32-3, cp32-5, and cp32-13, but less frequently for cp32-1 and cp32-10 (**Fig 5D**).

Additionally, 11.6% of reads > 5 kb mapped to the linear chromosome and ~6.3% of reads >5 kb mapped to lp54 (**Fig 5B**). The remaining reads mapped to all the defined genetic elements of *B. burgdorferi* CA-11.2A including plasmids cp26, lp17, lp36/lp28-4, lp38, lp56, and lp28-3 at 1–2% each (**Fig 5B**). *De novo* assembly of packaged reads produced full-length contigs of all cp32s, lp17, cp26, lp36, lp38, lp54, and lp56 (**Fig S1**), suggesting that full-length versions of these plasmids are packaged by ϕBB-1.

Of note, the CA-11.2A genome was reported to contain a unique plasmid, lp36/lp28-4, that is thought to have arisen from the fusion of lp36 with lp28-4 [48]. *De novo* assembly of packaged reads resolved lp36/lp28-4 into individual lp36 and lp28-4 contigs (**Fig S1E and F**). Additionally, whole genome sequencing of our CA-11.2A strain confirmed that lp36 and lp28-4 are separate as no reads that span the lp36-lp28-4 junction were observed and coverage depth was notably different between lp36 and lp28-4 (~200× vs. 25×, respectively, **Fig S2A**). Furthermore, PCR confirmed the sequencing results (**Fig S2B-D**). These data indicate that the lp36/lp28-4 plasmid is two distinct episomes in our CA-11.2A strain.

Collectively, these results indicate that in addition to cp32 molecules, ϕBB-1 is capable of packaging non-cp32 portions of the *B. burgdorferi* genome. We discuss the major packaged DNA species in the following sections.

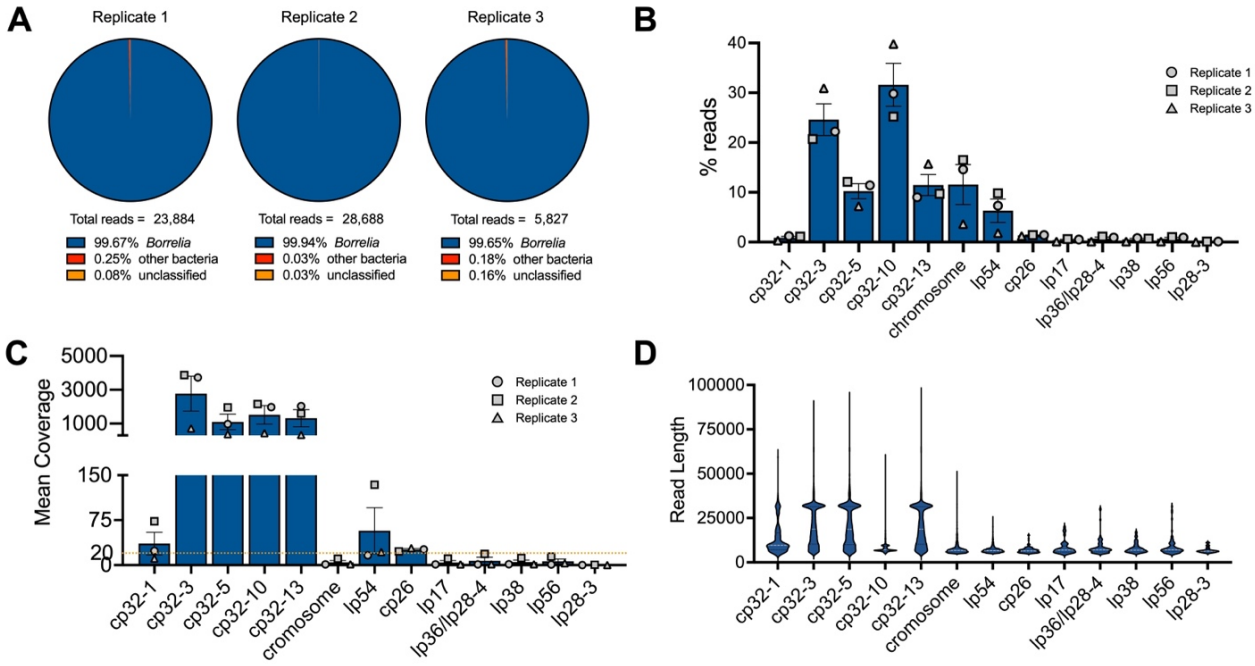

Figure 5. ϕBB-1 virions package cp32 isoforms, chromosome fragments, lp54, and other plasmid DNA. (A) Kraken and BLAST were used to determine the taxonomic affiliation of reads >5kb. Note that no eukaryotic reads were identified. **(B and C)** The (B) percent and (C) mean coverage for reads affiliated with the indicated *B. burgdorferi* plasmid or linear chromosome are shown for each replicate. Error bars represent the SE of the mean. **(D)** Read length distributions for the indicated plasmids or chromosome are shown.

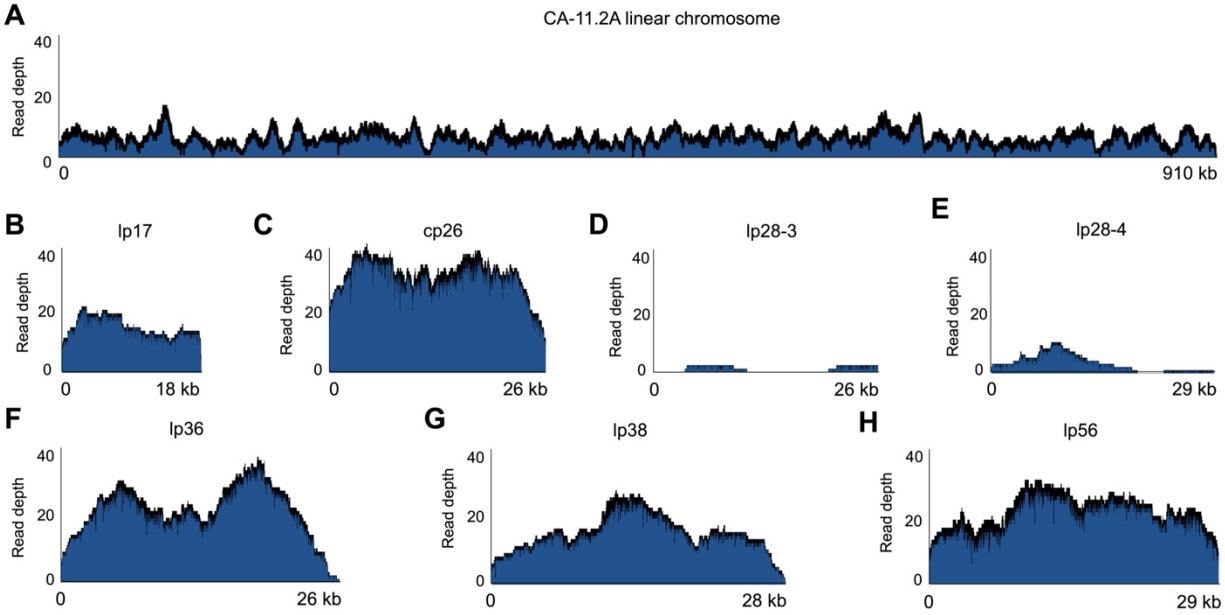

Figure S1. Packaged read depth across the *de novo* CA-11.2A genome assembly. *De novo* assembly of packaged reads >5kb produced the indicated contigs. Read coverage was then mapped to each contig. **(A–H)** Read coverage across the CA-11.2A chromosome or indicated plasmids are shown. Coverage maps for the cp32s and lp54 are shown in Figures 6 and 9, respectively.

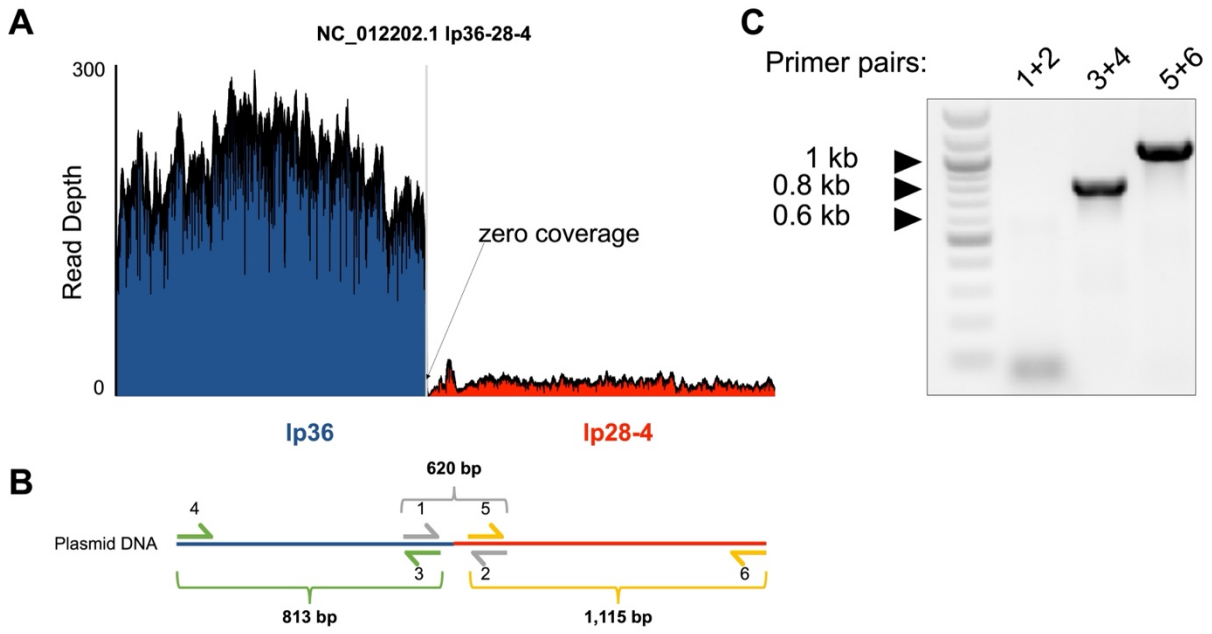

Figure S2. Whole genome sequencing of the CA-11.2A genome reveals that plasmid lp36/lp28-4 resolves into two separate episomes. (A) The CA-11.2A genome was sequenced using long-read technology. Reads were aligned to the lp36/lp28-4 reference sequence (NC_012202.1) and read depth plotted. **(B)** Schematic of PCR design. Primers 1 and 2 flank the lp36/lp28-4 junction, with primer 1 annealing to lp36 and primer 2 annealing to lp28-4, creating a 620 bp product if joined. Primers 3 and 4 anneal to lp36 DNA, creating an 813 bp product if present. Primers 5 and 6 anneal to lp28-4 DNA, creating a 1,115-bp product if present. **(C)** The presence or absence of lp36, lp28-4, or lp36/lp28-4 was confirmed by PCR.

<u>cp32 molecules are linearized near the *erp* locus and packaged via a headful mechanism</u>

Our sequencing data provide insight into how ϕBB-1 packages cp32 molecules. Many phage species package linear double-stranded DNA genomes that circularize after being injected into a host [49]. Because DNA isolated from ϕBB-1 virions is thought to be linearized [33], we used PhageTerm [50] to predict the linear ends of packaged DNA. Native DNA termini are present once per linear DNA molecule, but non-native DNA ends produced during sequencing are distributed randomly along DNA molecules. Thus, reads that start at native DNA terminal positions occur more frequently than anywhere else in the genome. PhageTerm takes advantage of this to resolve DNA termini and predict phage packaging mechanisms [50]. PhageTerm identified the termini of packaged cp32 molecules at approximately 26 kb in a region lying immediately upstream of the *erp* loci (**Fig 6A**). In agreement with the PhageTerm results, when packaged reads were used to map the physical ends of packaged cp32 molecules, a sharp boundary in coverage depth is observed upstream of the *erp* loci in all cp32s (**Fig 6B–F**). Notably, the intergenic region upstream of the *erp* loci is conserved across the cp32 isoforms found in diverse strains of Lyme disease spirochetes (**Fig 6G**) [15] and the linear cp32 ends identified by long-read sequencing converge at the same conserved terminal sequence motif (**Fig 6H**).

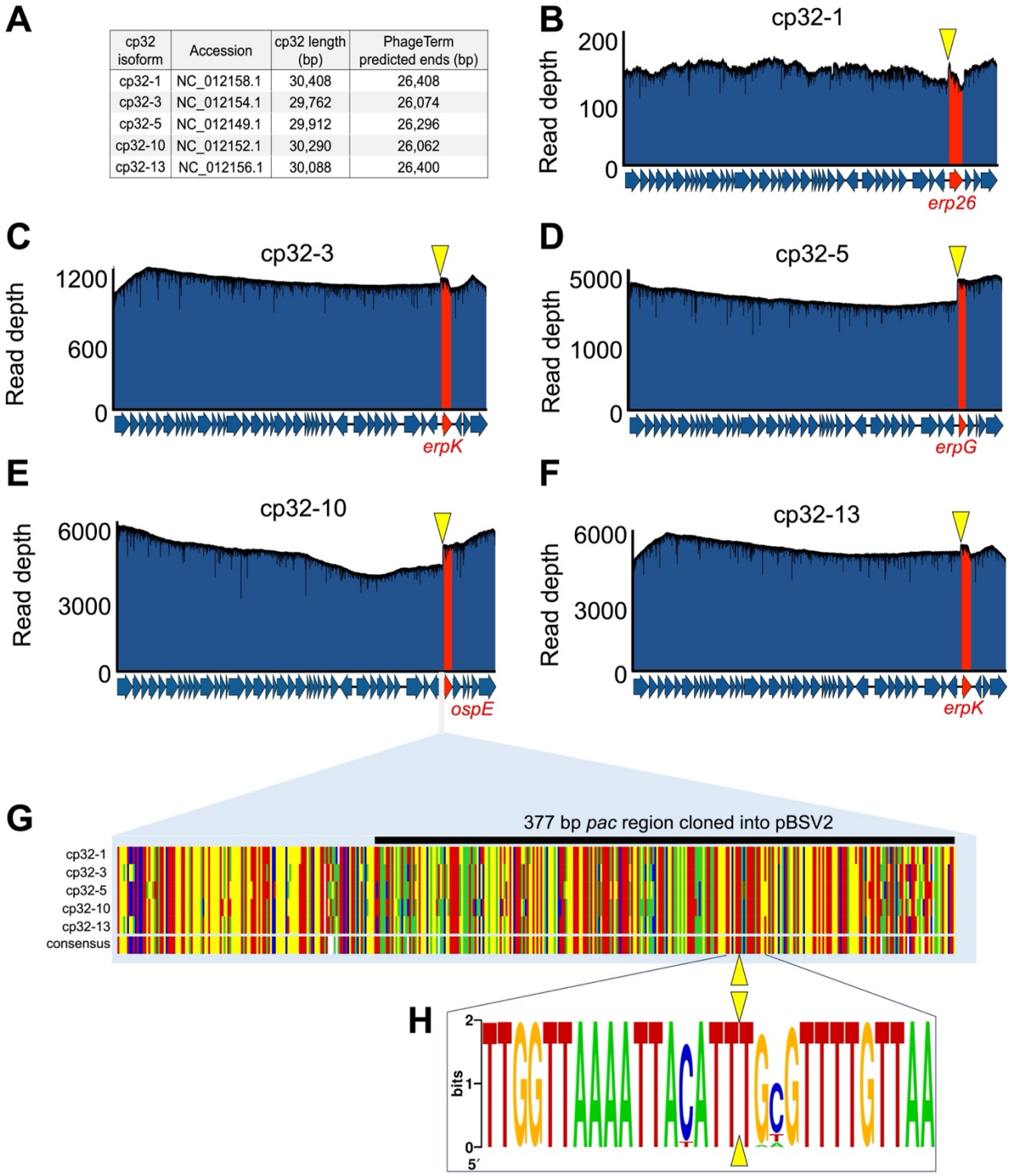

cp32 isoform	Accession	cp32 length (bp)	PhageTerm predicted ends (bp)
cp32-1	NC_012158.1	30,408	26,408
cp32-3	NC_012154.1	29,762	26,074
cp32-5	NC_012149.1	29,912	26,296
cp32-10	NC_012152.1	30,290	26,062
cp32-13	NC_012156.1	30,088	26,400

Fig 6. cp32s are linearized upstream of the *erp* loci. (A) PhageTerm was used to predict the linear ends of packaged cp32 molecules. **(B–F)** Nanopore reads were mapped to the indicated cp32s. Note the sharp boundary just upstream of the *erp* loci (highlighted in red). The yellow triangles indicate the PhageTerm predicted linear ends. **(G)** Alignments of the intergenic region upstream of the *erp* loci is shown for each cp32. Colors indicating A, T, C, or G are shown in panel H. The black line indicates the *pac* region that was cloned into a shuttle vector, as described in Figure 7. **(H)** A nucleic acid logo was constructed from 207 cp32 sequence alignments. Yellow triangles indicate the linear end of cp32 isoforms as predicted by PhageTerm and confirmed by long-read sequencing.

PhageTerm predicts that cp32s are packaged by a headful mechanism which supports the previously proposed headful genome packaging mechanism for cp32s [42].

231 Phages that use the headful packaging mechanism generate a concatemer containing
232 several head-to-tail copies of their genome (**Fig 7A**). During headful packaging, a cut is
233 made at a defined packaging site (*pac* site) and a headful (a little more than a full genome)
234 of linear phage DNA is packaged. Once a headful is achieved, the phage genome is cut
235 at non-defined sites, resulting in variable cut positions and size variation in packaged
236 DNA, which we observe in packaged cp32 reads downstream of the initial cut site (**Fig**
237 **6B–F**).

238 Our results suggest that the cp32 *pac* site is upstream of the *erp* loci. If the cp32
239 *pac* site is in this region, then DNA molecules containing the *pac* sequence are expected
240 to be packaged into ϕBB-1 virions. To test this, we cloned the putative cp32-3 *pac* site
241 (**Fig 6G**, black bar) into a derivative of the pBSV2 shuttle vector that lacks the promoter
242 and MCS [51], transformed *B. burgdorferi* strain CA-11.2A, and induced lytic ϕBB-1
243 replication with 5% ethanol. Supernatants containing virions were collected, filtered,
244 treated with chloroform, and DNase treated as described above. pBSV2 shuttle vector
245 copy numbers were measured by qPCR using primers that target the pBSV2 kanamycin
246 resistance (*kan*) cassette. To control for possible chromosomal DNA contamination,
247 qPCR was also performed using primers targeting the chromosomal *flaB* gene. Final
248 packaged pBSV2 copy numbers were calculated by subtracting *flaB* copy numbers from
249 pBSV2 (*kan* cassette) copy numbers.

250 Copy numbers of packaged pBSV2 encoding the cp32-3 *pac* site were significantly
251 (p<0.001) higher compared to virions collected from the supernatants of cells carrying an
252 empty pBSV2 vector (**Fig 7B**), indicating that DNA molecules that contain the *pac* site are
253 preferentially packaged by ϕBB-1 virions.

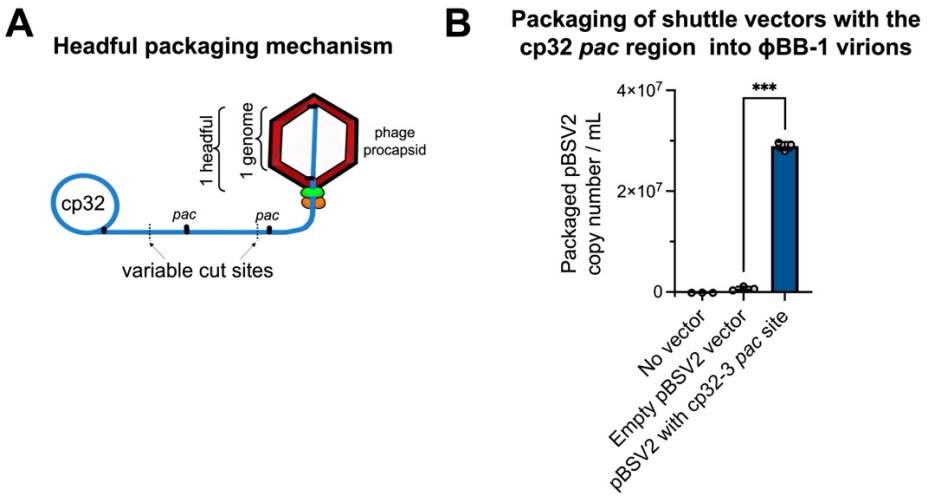

254

255 **Figure 7. Shuttle vectors containing the cp32 *pac* region are preferentially packaged into ϕBB-1**
256 **virions. (A)** Schematic depicting the headful genome packaging mechanism. **(B)** After ethanol induction,
257 ϕBB-1 virions were collected from CA-11.2A cells not carrying plasmid pBSV2 (No vector), cells
258 transformed with empty pBSV2, or cells transformed with pBSV2 with the cp32-3 *pac* site (see Fig 6G for
259 the cloned *pac* region). Copy numbers of pBSV2 packaged into ϕBB-1 virions were measured by qPCR.
260 Data are the SE of the mean of three experiments, ***p<0.001.

261 <u>The cp32 prophages have conserved motifs that occur in a specific arrangement not</u>
262 <u>found in other DNA sequences packaged by ϕBB-1 virions</u>

To identify motif(s) that may be shared between the cp32s and other genomic elements that are packaged into ϕBB-1 virions (*e.g.,* lp54), we first used an iterative BLAST search to identify distantly homologous DNA sequences (**Fig 8**). A non-redundant list of these diverse DNA sequences were then used as an input dataset for sequence motif discovery via MEME [52]. All five cp32 isoforms found in *B. burgdorferi* CA-11.2A have the same specific arrangement of conserved sequence motifs around the *pac* region (**Fig 8A and B**) and these are conserved in cp32 isoforms across *B. burgdorferi* (**Fig 8C**). However, significant matches to these motifs were not identified in other CA-11.2A genetic elements packaged by ϕBB-1 (**Supplementary Data file 1**), suggesting that packaging of non-cp32 DNA may occur spontaneously or through different mechanisms.

The complete or partial arrangement of motifs found around the *pac* site of *B. burgdorferi* cp32 isoforms is conserved in cp32 plasmids and some linear plasmids originating from other Lyme and relapsing fever *Borrelia* (21 species total) (**Fig. 8C**). The iterative BLAST search also revealed that a diverse set of circular and linear plasmids in a broader set of *Borrelia* species share some of the motifs found in *B. burgdorferi* cp32 isoforms. In total, linear or circular plasmid sequences from 21 different *Borrelia* species (both Lyme disease and relapsing fever spirochetes) had homology to the *B. burgdorferi* cp32 *pac*-containing DNA sequences (**Fig 8C**).

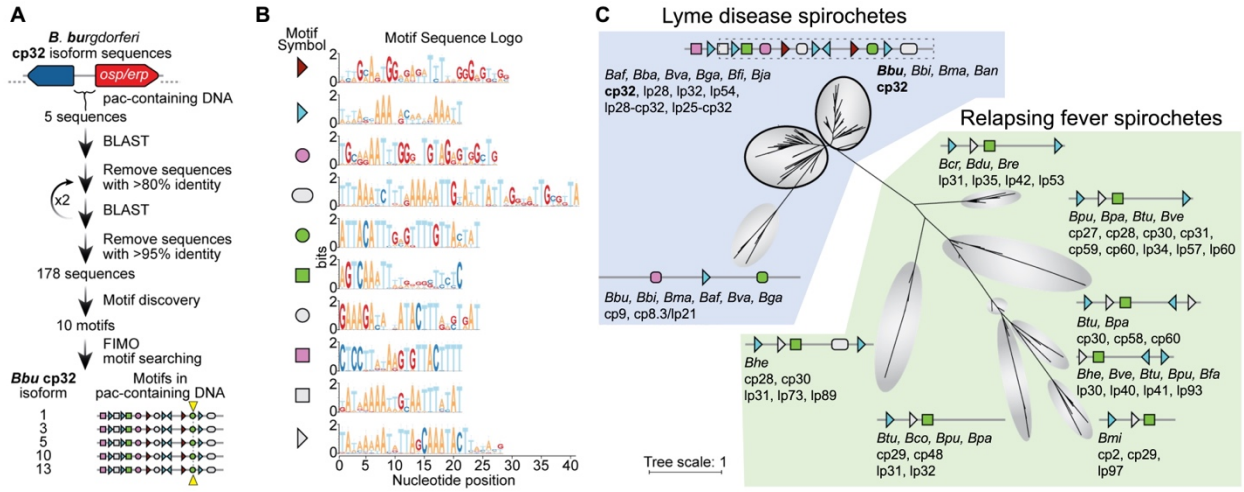

Figure 8. Cp32 prophages have conserved motifs that occur in a specific arrangement around the *pac* site. (A) Outline of bioinformatic strategy to identify motifs enriched in the *pac*-containing DNA sequence of cp32 isoforms. All *B. burgdorferi* cp32 isoforms have the same motifs in the *pac* region. The cp32 cut site is indicated by the yellow triangle. **(B)** Sequence logos of the motifs identified in panel A and schematized in panel C. Nine of the top ten motifs occur at least once in the *pac*-containing region of cp32 DNA sequences. Motifs represented with right or left facing triangles often occur as direct and/or indirect repeats. **(C)** Phylogenetic tree of non-redundant DNA sequences with homology to *B. burgdorferi* cp32 *pac*-region identified in panel A. For each clade, the bacterial species and type of plasmid are listed. For clarity in the figure, bacterial species names have been truncated to a three letter abbreviation consisting of the first letter of the genus and the first two letters of the species (*Borrelia afzelii, Baf; Borrelia andersonii, Ban; Borrelia bavariensis, Bba; Borrelia bissettiae, Bbi; Borrelia burgdorferi, Bbu; Borrelia coriaceae, Bco; Borrelia crocidurae, Bcr; Borrelia duttoni, Bdu; Borrelia fainii, Bfa; Borrelia finlandensis, Bfi; Borrelia garinii, Bga; Borrelia hermsii, Bhe; Borrelia japonica, Bja; Borrelia mayonii, Bma; Borrelia miyamotoi, Bmi; Borrelia parkeri, Bpa; Borrelia puertoricensis, Bpu; Borrelia recurrentis, Bre; Borrelia turicatae, Btu; Borrelia valaisiana, Bva; Borrelia venezuelensis, Bve*). There is variability in the motif architecture between

sequences within a single clade; however, for clarity, a representative motif architecture discovered by MEME is shown [52]. The top two clades of sequences (outlined in black) are dominated by cp32 isoforms and the cp32 motif architecture, therefore a single motif scheme is shown for these two clades. The region of DNA and motifs cloned into the pBSV2 shuttle vector is outlined in dashes.

Deciphering the structure of linear plasmids packaged by ϕBB-1

After the cp32s, lp54 is a major DNA species packaged by ϕBB-1 (**Fig 5C**). Lp54 is a linear plasmid with covalently closed telomeres that is present in all Lyme disease *Borrelia* with about a third of its encoded genes being paralogues to genes encoded on the cp32s [6, 53]. *De novo* assembly of packaged lp54 reads produces a 67.4 kb contig consisting of full-length lp54 (54,021 bp, NC_012194.1) flanked by sequences containing tail-to-tail (7,310 bp) and head-to-head (6,074 bp) junctions (**Fig 9A**). Read depth for lp54 was >100 for most of the contig; however, read depth drops precipitously at both tail-to-tail and head-to-head junctions (**Fig 9A**), suggesting that the telomeres of lp54 interfere with sequencing.

B. burgdorferi telomeres contain inverted repeat sequences [54] and we identified the CA-11.2A lp54 inverted repeat sequence as 5′–TTTATTAGTATACTAATAAA (**Fig 9B and C**, boxed sequences). Our sequencing of the telomeric ends of lp54 extends the reference sequence at the left telomeric end by seven nucleotides (**Fig 9B,** underlined). Further, compared to the lp54 reference sequence, the packaged left and right junction-spanning sequences each encode an additional 18 bp of sequence (**Fig 9B and C**). These sequences, although unique at each end (**Fig 9D**), form perfect hairpin structures (**Fig 9E and F**). Overall, these data suggest that lp54 molecules with complete telomere sequences are packaged into virions. However, whether linear lp54 with covalently closed telomeres or lp54 replication intermediates that contain head-to-head and tail-to-tail junctions are packaged is unclear.

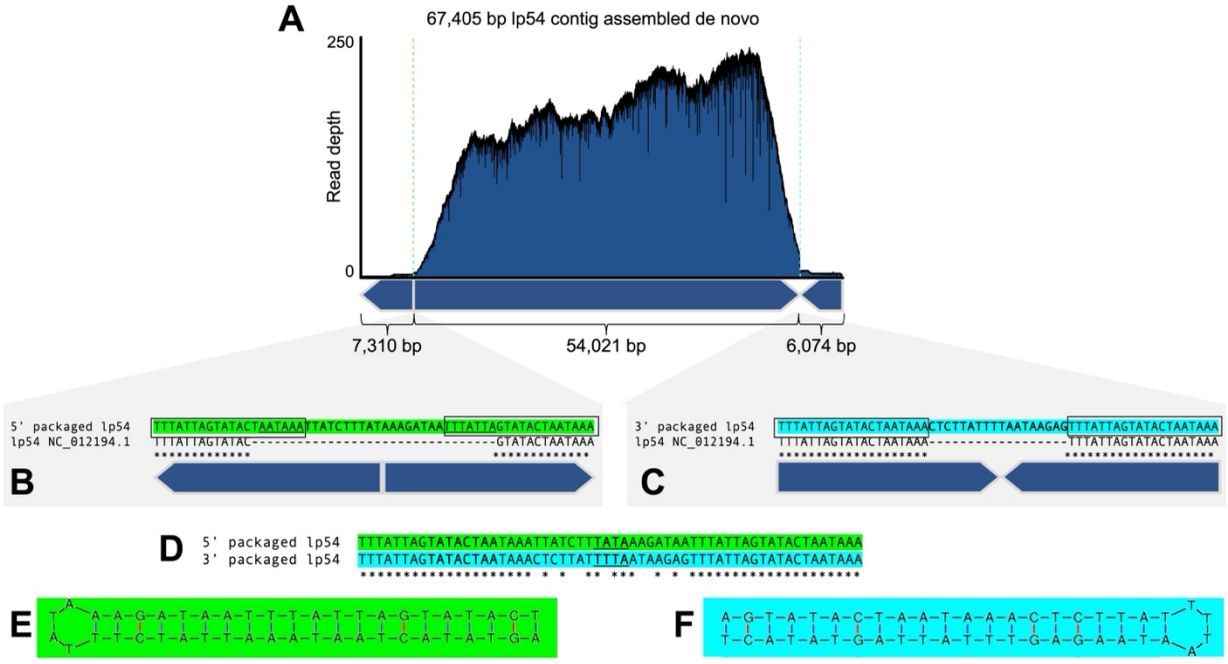

Figure 9. Full-length lp54 with fully resolved telomeres are recovered from ϕBB-1-packaged DNA. (A) *De novo* assembly of packaged reads produced a 67,405-bp contig with tail-to-tail and head-to-head

junctions. **(B and C)** Sequences at the packaged 5′ junction (green) or the 3′ junction (cyan) are compared to the lp54 reference sequence NC_012194.1. The conserved inverted repeat sequence 5′–TTTATTAGTATACTAATAAA is outlined. **(D)** Alignments of the tail-to-tail and head-to-head junctions reveals a variable 18-bp sequence in between the conserved inverted repeats. **(E and F)** Predicted hairpin structures are shown for each end of lp54. The loop sequence for each hairpin is underlined in panel D.

The *de novo* assembly approach applied to lp54 was also successful in resolving the telomeric ends of other linear elements of the CA-11.2A genome, including the linear chromosome and plasmids lp17, lp56, and lp38 (**Fig 10**). Additionally, we were able to resolve left and right telomeres for lp36 (**Fig 10**), providing yet further evidence that lp36 is not fused to lp28-4.

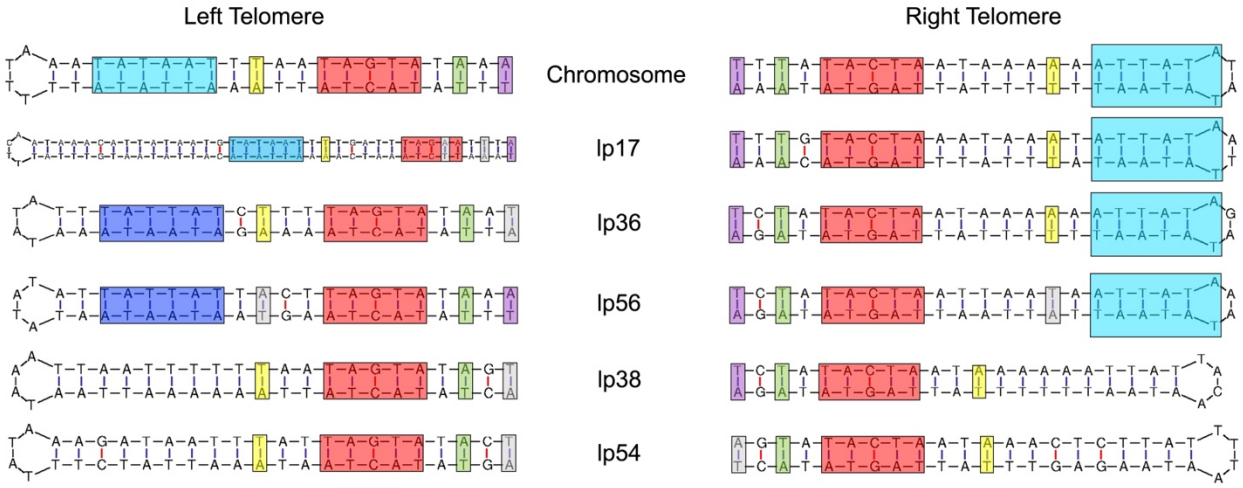

Figure 10. Packaged reads resolve the telomeric ends of the linear chromosome and most linear plasmids in the CA-11.2A genome. Reads spanning tail-to-tail or head-to-head junctions of the linear chromosome or the indicated linear plasmids form perfect hairpin structures. Conserved regulatory elements for each telomere are highlighted [55-60].

Discussion

In nature, Lyme disease spirochetes exist as diverse populations of closely related bacteria that possess sufficient antigenic variability to allow them to co-infect and reinfect non-naïve vertebrate hosts [61-72]. Moreover, horizontal gene transfer between Lyme disease spirochetes has been extensively documented [19, 73-77]. Nevertheless, the mechanism underlying horizontal genetic exchange among Lyme disease spirochetes has remained undefined. Our study implicates ϕBB-1 in mediating horizontal gene transfer between Lyme disease spirochetes.

Horizontal gene transfer between heterologous spirochetes likely occurs in the tick midgut during and immediately after a blood meal when spirochete replication rates and densities are at their highest. ϕBB-1 replication is also induced in the tick midgut during a bloodmeal [9, 30, 31] with implications for their facilitation of horizontal gene transfer evidenced by homologous recombination between cp32 isoforms [15-17] and the horizontal transfer of cp32s between *Borrelia* strains [21].

Our sequencing data indicate that ϕBB-1 virions package portions of the entire *B. burgdorferi* genome, giving ϕBB-1 the potential to mobilize numerous beneficial alleles during the enzootic cycle via generalized transduction. For example, the circular cp32 prophages are highly conserved across the *Borrelia* genus [26]; however, cp32 isoforms contain variable regions that encode outer membrane lipoproteins such as Bdr, Mlp, and OspE/OspF/Elp, which are known to facilitate the *B. burgdorferi* lifecycle [24, 26, 27, 78]. The linear plasmid lp54 encodes the outer membrane lipoproteins OspA and OspB, which are required for *B. burgdorferi* to colonize the tick midgut [79-81]. The outer membrane lipoprotein OspC, which is required for *B. burgdorferi* to infect a vertebrate host, is encoded by the circular plasmid cp26 [61, 76, 82]. These alleles (and many others) are packaged by ϕBB-1, which is consistent with a role for phage-mediated transduction of genes encoding essential membrane lipoproteins between heterologous spirochetes.

In *B. burgdorferi*, the linear chromosome is highly conserved as are the circular plasmids cp32 and cp26 and the linear plasmids lp17, lp38, lp54, and lp56 are all evolutionarily stable [4-6, 16, 83]. However, other plasmids distributed across the genospecies show considerably more variation, encode mostly (87%) pseudogenes, and are thought to be in a state of evolutionary decay [6]. The packaged plasmids for which we recovered full-length contigs include the cp32s, cp26, lp17, lp38, lp54, and lp56 —the same plasmids that are evolutionarily stable across the genospecies [4-6, 16, 83]. These observations suggest that genes encoded on ϕBB-1-packaged plasmids are under positive selection, possibly due to the continuous transduction between Lyme disease spirochetes during the enzootic cycle.

In addition to providing evidence that ϕBB-1 virions package large portions of the *B. burgdorferi* genome, our study provides insight into ϕBB-1 virion structure and identifies virion proteins present in ϕBB-1. Using mass spectrometry-based proteomics, we confirm that putative capsid and structural genes encoded by the cp32s, such as the major capsid protein P06, are indeed translated and assembled into mature ϕBB-1 virions.

382 Our long-read sequencing studies indicate that ϕBB-1 packages full-length linear
383 cp32 molecules via a headful mechanism using *pac* sites. The headful packaging
384 mechanism is used by numerous phages and was first described for *E. coli* phage T4 in
385 1967 [84]. After injecting linear DNA into a new host, the phage genome re-circularizes
386 before continuing its replication cycle. Genes encoded near the ends of linear phage
387 genomes are subject to copy number variation and recombination as the phage genome
388 re-circularizes [85]. Our data suggest that the conversion of linear cp32 molecules into
389 circular cp32 molecules occurs in the vicinity of the *erp* locus, which would facilitate
390 recombination with polymorphic *erp* alleles encoded by other cp32 isoforms in diverse *B.*
391 *burgdorferi* hosts.

392 In this study, the packaging of specific cp32 isoforms was biased: cp32-3, cp32-5,
393 cp32-10, and cp32-13 were predominantly packaged while cp32-1 was rarely packaged.
394 This result is consistent with observations by Wachter *et al.* where cp32 isoform copy
395 number and transcriptional activity were not uniform across all cp32 isoforms in *B.*
396 *burgdorferi* strain B31: cp32-1, cp32-3, and cp32-6 were predominantly induced (highest
397 copy numbers) and had the highest transcriptional activity while cp32-9 was not induced
398 and was transcriptionally inactive [9]. Variability in the *pac* region or other regulatory
399 elements involved in cp32 induction may explain why different cp32 isoforms replicate
400 and/or are packaged at different rates. On the other hand, the motifs that are found most
401 broadly in the *pac* region (*e.g.,* **Fig 8C**, blue triangle and green square) may represent
402 binding sites for conserved host factors that are present in all *Borrelia* species whereas
403 the other motifs may represent protein-binding sites or regulatory sequences that are
404 specific to given prophage or plasmids.

405 In the intergenic region upstream of the *erp* loci, we identified a 377-bp region that
406 contains the cp32 *pac* signal. Introducing the cp32 *pac* region to a shuttle vector facilitated
407 the packaging of the shuttle vector into ϕBB-1 virions. Our identification of the cp32 *pac*
408 site will be useful for the engineering of recombinant DNA that can be packaged into
409 virions that infect spirochetes, giving ϕBB-1 the potential for use as a tool for the genetic
410 dissection and manipulation of Lyme disease spirochetes.

411 After the cp32s, lp54 was the most frequently packaged plasmid. This may be
412 related to the evolutionary origins of lp54: about one-third of the genes encoded by lp54
413 are paralogous to cp32-encoded genes and lp54 is thought to have emerged from an
414 ancient recombination event between a cp32 and a linear plasmid [6]. In addition, lp54
415 encodes putative phage proteins including a porin (BBA74) [86] and phage capsid
416 proteins that are highly conserved across the genospecies [87], which we detected in
417 purified virions by mass spectrometry. While we observed virions with a distinct elongated
418 capsid morphology, virions with a notably smaller capsid morphology have been observed
419 after induction *in vitro* [9, 32, 33]. These observations raise the possibility that lp54 may
420 be a prophage, although it is not clear if lp54 produces its own capsids, relies on cp32-
421 encoded capsids, or if both lp54 and cp32 capsid proteins assemble to produce chimeric
422 virions.

423 Our long-read dataset contained reads that spanned head-to-head and tail-to-tail

junctions in lp54. These reads allowed us to define the lp54 telomere sequences; however, whether full-length lp54 molecules are packaged or at which stage of the replication cycle lp54 is packaged is unknown. In *B. burgdorferi*, both the linear chromosome and linear plasmids have covalently closed hairpin telomeres and replicate via a telomere resolution mechanism [56, 58, 88, 89]. Examination of a naturally occurring lp54 dimer in *B. valaisiana* isolate VS116 suggests that a circular head-to-head dimer is produced during lp54 replication prior to telomere resolution and replication completion [90]. Linear, covalently closed lp54 molecules may be packaged or lp54 replication intermediates may be packaged.

As obligate vector-borne bacteria, Lyme disease spirochetes live relatively restrictive lifestyles that might be expected to i) limit their exposure to novel gene pools, ii) enhance reductive evolution, and iii) favor the loss of mobile DNA elements. A role for ϕBB-1 in mediating the transduction of beneficial alleles between heterologous spirochetes in local vector and reservoir host populations may explain why cp32 prophages are ubiquitous not only among Lyme disease spirochetes, but also relapsing fever spirochetes.

Acknowledgments

We are grateful to Patti Rosa for helpful discussions and to the IDeA National Resource for Quantitative Proteomics Center at the University of Arkansas for their assistance with proteomic analyses of phage virions. PRS is supported by NIH grants R21AI151597 and P30GM140963. MK is supported by NIH grant P20GM103474. DRF is supported by NSF GRFP grant 366502. A.S-F. is a M. Jane Williams and Valerie Vargo Presidential Assistant Professor of Biology and is supported by NIH grants K99GM147842 and R00GM147842, and by the Postdoctoral Enrichment Program Award from the Burroughs Wellcome Fund (G-1021106.01). The funders had no role in study design, data collection and analysis, decision to publish, or preparation of the manuscript. The authors declare no conflicts of interest.

451 **Methods**

452 ϕBB-1 induction. *Borrelia burgdorferi* B31 or CA-11.2A was grown in BSK-II growth
453 medium to 7 × 10^7/mL and centrifuged at 6,000 × *g*, 10 min., 35°C to pellet cells, which
454 were resuspended in fresh media to a density of 2 × 10^8/mL. EtOH was added to a final
455 concentration of 5% and the resuspended culture was incubated at 35°C for an additional
456 2 hours to induce phage production. The induced culture was then centrifuged at 6,000 ×
457 *g*, 10 min, 35°C and the pellet was resuspended in fresh media to a density of 5 × 10^7/mL
458 after which it was incubated at 35°C for 72 hours to produce phage. After 72 hours, the
459 culture was centrifuged at 6,000 × *g* for 10 min to remove cells and the phage-containing
460 supernatant was filtered twice through 0.2 µm filters before storage at 4°C.

461 cp32 qPCR. For qPCR, 100 µL of filtered culture supernatant was mixed with 20ul of
462 chloroform to eliminate remaining intact cells and then centrifuged to separate the
463 phases. 80 µL of the aqueous phase was transferred to a new tube, mixed with 0.8 µL of
464 100X DNaseI reaction buffer (1M Tris-HCl pH 7.5, 250 mM $MgCl_2$, 50 mM $CaCl_2$) and
465 DNase treated with 0.8U DNaseI for 1 hour at 37°C. Following DNase treatment,
466 supernatants were mixed with 20 µl chloroform to inactivate DNase, spun to separate
467 phases and the aqueous phase added directly to a qPCR reaction (0.5 µL treated
468 supernatant/10 µL total reaction volume). qPCR was performed using SsoAdvanced
469 Universal Inhibitor-Tolerant SYBR green supermix (BioRad, Hercules, CA) following
470 maufacturer's instructions, primers that target a conserved cp32 intergenic region
471 between *bbp08* and *bbp09* (5'-CTTTACACATATCAAGACCTTAAC, 5'-
472 CAAACCACCCAATTTCCAATTCC) and the *flaB* gene to control for *B. burgdorferi*
473 chromosomal DNA contamination (5'-TCTTTTCTCTGGTGAGGGAGCT, 5'-
474 TCCTTCCTGTTGAACACCCTCT) [91] at an empirically determined annealing
475 temperature of 55°C. Absolute cp32 and *flaB* copy numbers were calculated from a
476 standard curve generated using a cloned copy of the target sequences. To estimate
477 phage number for CA-11.2A and correct for any remaining unpackaged cp32 plasmids,
478 five times the number of detected *flaB* copies was subtracted from the absolute cp32
479 starting quantity.

480 ϕBB-1 virion purification for DNA extraction. Centrifuged, filtered phage supernatants
481 were treated with 1/10th volume of chloroform to lyse any remaining cells and chloroform
482 was allowed to separate at 4ºC overnight. The aqueous layer was transferred to a new
483 vessel and mixed with saturated ammonium sulfate to a final concentration of 50%. NaOH
484 was slowly added during ammonium sulfate addition to maintain pH based on the BSK-II
485 phenol red indicator and the final pH was adjusted to 7.5. Precipitations were incubated
486 overnight 4ºC and then centrifuged at 10,000 × g for 30 minutes (4ºC) to collect phage
487 pellets. Precipitated phages were gently resuspended in SM buffer overnight at 4ºC.

488 ϕBB-1 electron microscopy imaging. Purified virions (3–4 µl) were absorbed to the surface
489 of freshly glow-discharged, formvar-coated 200 mesh copper grids and negatively stained
490 with 5 µl of 2% methylamine vanadate (Nanoprobes, Yaphank, NY) prior to viewing on a
491 Hitachi HT7700 transmission electron microscope (Hitachi-High-Technologies
492 Corporation, Tokyo, Japan).

493 ϕBB-1 virion proteomics. Purified virions (200 µg total protein) were reduced, alkylated,
494 and purified by chloroform/methanol extraction prior to digestion with sequencing grade
495 modified porcine trypsin (Promega). Peptides were separated on an Acquity BEH C18
496 column (100 x 1.0 mm, Waters) using an UltiMate 3000 UHPLC system (Thermo).
497 Peptides were eluted by a 50 min gradient from 99:1 to 60:40 buffer A:B ratio (Buffer A =
498 0.1% formic acid, 0.5% acetonitrile. Buffer B = 0.1% formic acid, 99.9% acetonitrile).
499 Eluted peptides were ionized by electrospray (2.4 kV) followed by mass spectrometric
500 analysis on an Orbitrap Eclipse Tribrid mass spectrometer (Thermo) using multi-notch
501 MS3 parameters. MS data were acquired using the FTMS analyzer over a range of 375
502 to 1500 m/z. Up to 10 MS/MS precursors were selected for HCD activation with
503 normalized collision energy of 65 kV, followed by acquisition of MS3 reporter ion data
504 using the FTMS analyzer over a range of 100-500 m/z. Proteins were identified and
505 quantified using MaxQuant (Max Planck Institute) TMT MS3 reporter ion quantification
506 with a parent ion tolerance of 2.5 ppm and a fragment ion tolerance of 0.5 Da.

507 Packaged ϕBB-1 DNA purification. For DNA extractions, phage were collected and
508 precipitated as described above, with the addition of a DNase treatment prior to
509 ammonium precipitation. The aqueous phage of chloroform supernatants were mixed with
510 1/100th volume 100X DNAse buffer and 1U/mL DNase I followed by incubated at 37°C for
511 3 hours and by 4°C overnight. For samples subjected to population sequencing, high
512 molecular-weight salmon sperm DNA (1.7 µg/mL, a concentration that approximates the
513 amount of DNA released by 3×10^8 lysed bacterial cells per milliliter of media) was added
514 prior to DNAse digestion to assess carryover of DNA contained outside of phage capsids.

515 After ammonium sulfate precipitation and resuspension of phage pellets in SM
516 buffer, EDTA was added to a final concentration of 5 mM and SDS to a final concentration
517 of 0.5%. After addition of 20 µg/mL RNAse and incubation at room temperature for 20
518 minutes, phage capsids were digested with 200ug/mL proteinase K at 55°C for 1 hour.
519 Samples were extracted twice with an equal volume of phenol-chloroform-isoamyl alcohol
520 (25:24:1) followed by a single extraction with an equal volume of chloroform-isoamyl
521 alcohol (24:1) using Qiagen Maxtract High Density medium (Qiagen, Hilden, Germany).
522 NaCl was added to 300 mM and DNA was precipitated with 2.5 volumes of 100% EtOH
523 at -20°C overnight. DNA was pelleted by centrifugation (14,000 × g for 20 min at 4°C),
524 washed 3X with 70% EtOH and re-spun for 20 min, at 14,000 × g 4°C. The DNA pellet
525 was gently air-dried followed by resuspension in 10mM Tris-HCl, pH 8.5 at 4°C overnight.

526 Nanopore sequencing. Sequencing libraries were prepared according to manufacturer's
527 instructions using library kit SQK-LSK112, native barcoding kit SQK-NBD112.24 and 500
528 ng of purified phage DNA (Oxoford Nanopore, Oxford, UK). Libraries were sequenced on
529 a MinION MK1-B using a FLO-MIN112 flowcell and default settings until pores were
530 exhausted. Basecalling and demultiplexing was performed with Guppy 6.4.6 using the
531 super high accuracy (SUP) model (dna_r10.4_e8.1_sup.cfg) and default parameters.
532 Run quality control measures were checked with MinIONQC (v1.4.1) [92] and FastQC
533 (v0.11.9). Adaptor trimming was performed using s (v0.2.4) [93]. Reads were deposited
534 in the NCBI BioProject database accession PRJNA1059007 and in Supplementary Data

File 2.

Sequence analysis pipeline. Adapter-trimmed long-reads with quality scores ≥7 were used to isolate ≥ 5kb reads using Filtlong (v0.2.1). ≥5kb reads were mapped to the reference *B. burgdorferi* CA-11.2A genome (RefSeq assembly: GCF_000172315.2) with minimap2 (v2.26-r1175) [94]. Primary mapping reads with MAPQ >20 were isolated by contig, filtered, and converted to final file formats using Samtools (v1.17) [95] and SeqKit (v2.5.1) [96]. Read statistics for each replicate were graphed and viewed using GraphPad Prism (v10.1.1). For each contig, *de novo* assemblies were created using Trycycler (v0.5.4) [97], which relied on input assemblies from Flye (v2.9.2-b1786) [98], Raven (v1.8.3) [99], and Minimap2/Miniasm/Minipolish (v2.26-r1175/v0.3-r179/v0.1.2) [94, 100]. The long-read *de novo* assemblies were then polished with short reads using Minipolish (v0.1.2) [100]. The telomeres of the linear chromosome and linear plasmids were manually identified in SnapGene (v5.3.3), and the hairpin structures were predicted by the Mfold webserver (http://www.unafold.org/mfold/applications/dna-folding-form.php) [101]. The terminal ends of the cp32 prophage genomes were predicted using PhageTerm through the Galaxy webserver (https://galaxy.pasteur.fr/) [50], via input of the ≥5kb long-read sequences. Coverage maps of the primary mapping or primary and supplementary mapping reads were created by mapping ≥ 5kb long-reads to the *de novo* assembled CA-11.2A genome or the reference *B. burgdorferi* CA-11.2A genome with Minimap2, converted to final file formats using Samtools, and viewed using R (v4.3.2) and ggplot2 (v3.4.4).

Pac site cloning and qPCR. The putative *pac* region from CA-11.2A genomic DNA was amplified using primers 5'-TAGACATGAGCGGCCGCAAGACAAGCTCCTTATAAGTGTTACT-3' and 5'-ATAGCTAGATGCGGCCGCTTACTCCGTAACTCTAAAGAATAATGC-3', purified and digested with NotI and cloned into Not-I-digested pBSV2_2 [51] to create a shuttle vector in which the CA-11.2A *pac* region is maintained but cannot be expressed. Vector sequences were verified using long-read sequencing and transformed into CA-11.2A via electroporation [102]. Clones were PCR-screened for maintenance of resident plasmids as previously described using published primers for *B. burgdorferi* cp32-1, cp26, cp32-3 (which target CA-11.2A cp32-5), cp32-6 (which target CA-11.2A cp32-3), lp28-3, lp17, lp54, lp28-4 [103] and CA-11.2A-specific primers for cp32-3 (5'-TGGGTTGTAGAGTGGCTGTG-3', 5'-TCACCACTTGCGTAATTCTTGC-3'), cp32-10 (5'-TAGAGCAAAGTCTTGAAAAGACAAC-3', 5'-CCCACGCTTTGTTGAGACC-3') and cp32-13 (5'- AATCTGGGCTGTAGAGCAGG-3', 5'-CTGCTCCTGAGGCTCATCC-3'). Clones transformed with *pac* plasmids or the empty vector were grown in triplicate to late-log phase in BSK-II and used to generate phage as described above. Encapsidated vector was measured directly from DNase-treated culture supernatants as described above using qPCR primers that target the *kan* resistance gene on pBSV2_2 (5'-CACCGGATTCAGTCGTCACT-3', 5'-GATCCTGGTATCGGTCTGCG-3', 120 bp product). A cloned copy of the *kan* PCR product was used to generate a standard curve for absolute quantification.

577 Identification of conserved motifs in *B. burgdorferi* cp32 isoforms. The roughly 430
578 nucleotides upstream of the *erp26*, *erpK*, *erpG*, *ospE* and *erpK* genes of the *B. burgdorferi*
579 CA-11.2A cp32 isoforms cp32-1, cp32-3, cp32-5, cp32-10 and cp32-13 respectively were
580 used as queries for a discontinuous MegaBLAST against the NCBI Nucleotide collection
581 database. The results from these first five BLASTs were combined and sequence hits
582 with more than 80% identity were removed with CD-HIT [104]. The resulting
583 representative sequences were used as queries for discontinuous MegaBLAST against
584 the NCBI Nucleotide collection (nt) database, and sequence hits with more than 80%
585 identity were removed with CD-HIT [104]. This process was iterated twice more for a total
586 of three MegaBLAST searches with a representative list of 80% identity query sequences.
587 The sequence hits from the final MegaBLASTs were combined and sequences with more
588 than 95% identity were removed with CD-HIT [104], generating a list of 178 sequences.
589 These 178 sequences were used as an input dataset for the MEME webserver [52], with
590 custom parameters of "Maximum Number of Motifs" set to "10", and "Motif Site
591 Distribution" set to "Any number of sites per sequence". MEME identified motifs in 160 of
592 the input sequences. The Position Weight Matrices (PWMs) of the 10 motifs identified by
593 MEME were used as inputs for FIMO [105] to search for significant sequence matches
594 (q-value < 0.001) in the *B. burgdorferi* chromosome and the *B. burgdorferi* cp32-1, cp32-
595 3, cp32-5, cp32-10, cp32-13, cp26, lp17, lp54 plasmid DNA sequences. The cp32
596 isoforms had nine highly conserved sequence motifs, some motifs present in multiple
597 copies and arranged in a conserved architecture. The cp26, lp17, lp54 and chromosome
598 sequences did not contain this conserved architecture of nine motifs (see Supplementary
599 Data file 1). The sequence logo of each motif was generated by taking the sequence
600 fragments that MEME used to make each PWM, and submitting these sequence
601 fragments to the WebLogo 3.0 webserver [106]. The iterative discontinuous MegaBLAST
602 searches had introduced eukaryotic sequence fragments into the list of 178 non-
603 redundant sequences, suggesting that the search likely reached an endpoint and found
604 most of the related sequences in the NCBI database. To generate a phylogenetic tree,
605 eukaryotic sequence fragments were first removed, and the remaining 149 non-redundant
606 sequences were aligned using the MAFFT webserver [107], with custom parameters of
607 "Direction of nucleotide sequences" set to "Adjust direction according to the first
608 sequence", and "Strategy" set to E-INS-2. The resulting alignment was used as input for
609 the IQ-TREE webserver [108, 109], with the following command-line: path_to_iqtree -s
610 *.fasta -st DNA -m TEST -bb 1000 -alrt 1000. TreeViewer was used to display the
611 phylogenetic tree [110].

References

1. Mead PS. Epidemiology of Lyme disease. Infect Dis Clin North Am. 2015;29(2):187-210. Epub 2015/05/23. doi: 10.1016/j.idc.2015.02.010. PubMed PMID: 25999219.
2. Adrion ER, Aucott J, Lemke KW, Weiner JP. Health care costs, utilization and patterns of care following Lyme disease. PLoS One. 2015;10(2):e0116767. Epub 2015/02/05. doi: 10.1371/journal.pone.0116767. PubMed PMID: 25650808; PubMed Central PMCID: PMC4317177.
3. Radolf JD, Strle K, Lemieux JE, Strle F. Lyme Disease in Humans. Curr Issues Mol Biol. 2021;42:333-84. Epub 20201211. doi: 10.21775/cimb.042.333. PubMed PMID: 33303701; PubMed Central PMCID: PMCPMC7946767.
4. Schwartz I, Margos G, Casjens SR, Qiu WG, Eggers CH. Multipartite Genome of Lyme Disease Borrelia: Structure, Variation and Prophages. Curr Issues Mol Biol. 2021;42:409-54. Epub 20201217. doi: 10.21775/cimb.042.409. PubMed PMID: 33328355.
5. Casjens SR, Mongodin EF, Qiu WG, Luft BJ, Schutzer SE, Gilcrease EB, et al. Genome stability of Lyme disease spirochetes: comparative genomics of Borrelia burgdorferi plasmids. PLoS One. 2012;7(3):e33280. Epub 20120314. doi: 10.1371/journal.pone.0033280. PubMed PMID: 22432010; PubMed Central PMCID: PMCPMC3303823.
6. Casjens S, Palmer N, van Vugt R, Huang WM, Stevenson B, Rosa P, et al. A bacterial genome in flux: the twelve linear and nine circular extrachromosomal DNAs in an infectious isolate of the Lyme disease spirochete Borrelia burgdorferi. Mol Microbiol. 2000;35(3):490-516. Epub 2000/02/15. PubMed PMID: 10672174.
7. Samuels DS, Lybecker MC, Yang XF, Ouyang Z, Bourret TJ, Boyle WK, et al. Gene Regulation and Transcriptomics. Curr Issues Mol Biol. 2021;42:223-66. Epub 20201210. doi: 10.21775/cimb.042.223. PubMed PMID: 33300497; PubMed Central PMCID: PMCPMC7946783.
8. Fraser CM, Casjens S, Huang WM, Sutton GG, Clayton R, Lathigra R, et al. Genomic sequence of a Lyme disease spirochaete, Borrelia burgdorferi. Nature. 1997;390(6660):580-6. doi: 10.1038/37551. PubMed PMID: 9403685.
9. Wachter J, Cheff B, Hillman C, Carracoi V, Dorward DW, Martens C, et al. Coupled induction of prophage and virulence factors during tick transmission of the Lyme disease spirochete. Nat Commun. 2023;14(1):198. Epub 20230113. doi: 10.1038/s41467-023-35897-3. PubMed PMID: 36639656; PubMed Central PMCID: PMCPMC9839762.
10. Qiu WG, Martin CL. Evolutionary genomics of Borrelia burgdorferi sensu lato: findings, hypotheses, and the rise of hybrids. Infect Genet Evol. 2014;27:576-93. Epub 20140403. doi: 10.1016/j.meegid.2014.03.025. PubMed PMID: 24704760; PubMed Central PMCID: PMCPMC4299872.
11. Brisson D, Drecktrah D, Eggers CH, Samuels DS. Genetics of Borrelia burgdorferi. Annu Rev Genet. 2012;46:515-36. Epub 2012/09/15. doi: 10.1146/annurev-genet-011112-112140. PubMed PMID: 22974303; PubMed Central PMCID: PMCPMC3856702.
12. Qiu WG, Bosler EM, Campbell JR, Ugine GD, Wang IN, Luft BJ, et al. A population genetic study of Borrelia burgdorferi sensu stricto from eastern Long Island, New York, suggested frequency-dependent selection, gene flow and host adaptation. Hereditas. 1997;127(3):203-16. doi: 10.1111/j.1601-5223.1997.00203.x. PubMed PMID: 9474903.
13. Haven J, Vargas LC, Mongodin EF, Xue V, Hernandez Y, Pagan P, et al. Pervasive recombination and sympatric genome diversification driven by frequency-dependent

661 selection in Borrelia burgdorferi, the Lyme disease bacterium. Genetics.
662 2011;189(3):951-66. Epub 20110902. doi: 10.1534/genetics.111.130773. PubMed PMID:
663 21890743; PubMed Central PMCID: PMCPMC3213364.
664 14. Combs MA, Tufts DM, Adams B, Lin YP, Kolokotronis SO, Diuk-Wasser MA. Host
665 adaptation drives genetic diversity in a vector-borne disease system. PNAS Nexus.
666 2023;2(8):pgad234. Epub 20230808. doi: 10.1093/pnasnexus/pgad234. PubMed PMID:
667 37559749; PubMed Central PMCID: PMCPMC10408703.
668 15. Brisson D, Zhou W, Jutras BL, Casjens S, Stevenson B. Distribution of cp32
669 prophages among Lyme disease-causing spirochetes and natural diversity of their
670 lipoprotein-encoding erp loci. Appl Environ Microbiol. 2013;79(13):4115-28. Epub
671 20130426. doi: 10.1128/AEM.00817-13. PubMed PMID: 23624478; PubMed Central
672 PMCID: PMCPMC3697573.
673 16. Casjens SR, Gilcrease EB, Vujadinovic M, Mongodin EF, Luft BJ, Schutzer SE, et
674 al. Plasmid diversity and phylogenetic consistency in the Lyme disease agent Borrelia
675 burgdorferi. BMC Genomics. 2017;18(1):165. Epub 20170215. doi: 10.1186/s12864-017-
676 3553-5. PubMed PMID: 28201991; PubMed Central PMCID: PMCPMC5310021.
677 17. Margos G, Hepner S, Mang C, Marosevic D, Reynolds SE, Krebs S, et al. Lost in
678 plasmids: next generation sequencing and the complex genome of the tick-borne
679 pathogen Borrelia burgdorferi. BMC Genomics. 2017;18(1):422. Epub 2017/06/01. doi:
680 10.1186/s12864-017-3804-5. PubMed PMID: 28558786; PubMed Central PMCID:
681 PMCPMC5450258.
682 18. Barbour AG, Travinsky B. Evolution and distribution of the ospC Gene, a
683 transferable serotype determinant of Borrelia burgdorferi. MBio. 2010;1(4). Epub
684 20100928. doi: 10.1128/mBio.00153-10. PubMed PMID: 20877579; PubMed Central
685 PMCID: PMCPMC2945197.
686 19. Marconi RT, Samuels DS, Landry RK, Garon CF. Analysis of the distribution and
687 molecular heterogeneity of the ospD gene among the Lyme disease spirochetes:
688 evidence for lateral gene exchange. J Bacteriol. 1994;176(15):4572-82. doi:
689 10.1128/jb.176.15.4572-4582.1994. PubMed PMID: 7913928; PubMed Central PMCID:
690 PMCPMC196277.
691 20. Stevenson B, Casjens S, Rosa P. Evidence of past recombination events among
692 the genes encoding the Erp antigens of Borrelia burgdorferi. Microbiology (Reading).
693 1998;144 (Pt 7):1869-79. doi: 10.1099/00221287-144-7-1869. PubMed PMID: 9695920.
694 21. Stevenson B, Miller JC. Intra- and interbacterial genetic exchange of Lyme disease
695 spirochete erp genes generates sequence identity amidst diversity. J Mol Evol.
696 2003;57(3):309-24. Epub 2003/11/25. doi: 10.1007/s00239-003-2482-x. PubMed PMID:
697 14629041.
698 22. Touchon M, Moura de Sousa JA, Rocha EP. Embracing the enemy: the
699 diversification of microbial gene repertoires by phage-mediated horizontal gene transfer.
700 Curr Opin Microbiol. 2017;38:66-73. Epub 20170517. doi: 10.1016/j.mib.2017.04.010.
701 PubMed PMID: 28527384.
702 23. Brissette CA, Haupt K, Barthel D, Cooley AE, Bowman A, Skerka C, et al. Borrelia
703 burgdorferi infection-associated surface proteins ErpP, ErpA, and ErpC bind human
704 plasminogen. Infect Immun. 2009;77(1):300-6. Epub 2008/11/13. doi: 10.1128/IAI.01133-
705 08. PubMed PMID: 19001079; PubMed Central PMCID: PMCPMC2612283.
706 24. Brissette CA, Cooley AE, Burns LH, Riley SP, Verma A, Woodman ME, et al. Lyme
707 borreliosis spirochete Erp proteins, their known host ligands, and potential roles in
708 mammalian infection. Int J Med Microbiol. 2008;298 Suppl 1:257-67. Epub 20080111.
709 doi: 10.1016/j.ijmm.2007.09.004. PubMed PMID: 18248770; PubMed Central PMCID:
710 PMCPMC2596196.

711 25. Stevenson B, Bono JL, Schwan TG, Rosa P. Borrelia burgdorferi erp proteins are
712 immunogenic in mammals infected by tick bite, and their synthesis is inducible in cultured
713 bacteria. Infect Immun. 1998;66(6):2648-54. Epub 1998/05/29. doi:
714 10.1128/IAI.66.6.2648-2654.1998. PubMed PMID: 9596729; PubMed Central PMCID:
715 PMCPMC108251.
716 26. Stevenson B, Zuckert WR, Akins DR. Repetition, conservation, and variation: the
717 multiple cp32 plasmids of Borrelia species. J Mol Microbiol Biotechnol. 2000;2(4):411-22.
718 Epub 2000/11/15. PubMed PMID: 11075913.
719 27. Kenedy MR, Lenhart TR, Akins DR. The role of Borrelia burgdorferi outer surface
720 proteins. FEMS Immunol Med Microbiol. 2012;66(1):1-19. Epub 20120521. doi:
721 10.1111/j.1574-695X.2012.00980.x. PubMed PMID: 22540535; PubMed Central PMCID:
722 PMCPMC3424381.
723 28. Stevenson B, Casjens S, Rosa P. Evidence of past recombination events among
724 the genes encoding the Erp antigens of Borrelia burgdorferi. Microbiology (Reading).
725 1998;144 (Pt 7):1869-79. doi: 10.1099/00221287-144-7-1869. PubMed PMID: 9695920.
726 29. Qiu WG, Schutzer SE, Bruno JF, Attie O, Xu Y, Dunn JJ, et al. Genetic exchange
727 and plasmid transfers in Borrelia burgdorferi sensu stricto revealed by three-way genome
728 comparisons and multilocus sequence typing. Proc Natl Acad Sci U S A.
729 2004;101(39):14150-5. Epub 20040916. doi: 10.1073/pnas.0402745101. PubMed PMID:
730 15375210; PubMed Central PMCID: PMCPMC521097.
731 30. Sapiro AL, Hayes BM, Volk RF, Zhang JY, Brooks DM, Martyn C, et al.
732 Longitudinal map of transcriptome changes in the Lyme pathogen Borrelia burgdorferi
733 during tick-borne transmission. Elife. 2023;12. Epub 20230714. doi: 10.7554/eLife.86636.
734 PubMed PMID: 37449477.
735 31. Tokarz R, Anderton JM, Katona LI, Benach JL. Combined effects of blood and
736 temperature shift on Borrelia burgdorferi gene expression as determined by whole
737 genome DNA array. Infect Immun. 2004;72(9):5419-32. doi: 10.1128/IAI.72.9.5419-
738 5432.2004. PubMed PMID: 15322040; PubMed Central PMCID: PMCPMC517457.
739 32. Eggers CH, Kimmel BJ, Bono JL, Elias AF, Rosa P, Samuels DS. Transduction by
740 phiBB-1, a bacteriophage of Borrelia burgdorferi. J Bacteriol. 2001;183(16):4771-8. doi:
741 10.1128/JB.183.16.4771-4778.2001. PubMed PMID: 11466280; PubMed Central
742 PMCID: PMCPMC99531.
743 33. Eggers CH, Samuels DS. Molecular evidence for a new bacteriophage of Borrelia
744 burgdorferi. J Bacteriol. 1999;181(23):7308-13. Epub 1999/11/26. PubMed PMID:
745 10572135; PubMed Central PMCID: PMCPMC103694.
746 34. Zhang H, Marconi RT. Demonstration of cotranscription and 1-methyl-3-nitroso-
747 nitroguanidine induction of a 30-gene operon of Borrelia burgdorferi: evidence that the
748 32-kilobase circular plasmids are prophages. J Bacteriol. 2005;187(23):7985-95. Epub
749 2005/11/18. doi: 10.1128/JB.187.23.7985-7995.2005. PubMed PMID: 16291672;
750 PubMed Central PMCID: PMCPMC1291276.
751 35. Fillol-Salom A, Alsaadi A, Sousa JAM, Zhong L, Foster KR, Rocha EPC, et al.
752 Bacteriophages benefit from generalized transduction. PLoS Pathog.
753 2019;15(7):e1007888. Epub 2019/07/06. doi: 10.1371/journal.ppat.1007888. PubMed
754 PMID: 31276485; PubMed Central PMCID: PMCPMC6636781.
755 36. Zinder ND, Lederberg J. Genetic exchange in Salmonella. J Bacteriol.
756 1952;64(5):679-99. doi: 10.1128/jb.64.5.679-699.1952. PubMed PMID: 12999698;
757 PubMed Central PMCID: PMCPMC169409.
758 37. Budzik JM, Rosche WA, Rietsch A, O'Toole GA. Isolation and characterization of
759 a generalized transducing phage for Pseudomonas aeruginosa strains PAO1 and PA14.

760 J Bacteriol. 2004;186(10):3270-3. Epub 2004/05/06. doi: 10.1128/JB.186.10.3270-
761 3273.2004. PubMed PMID: 15126493; PubMed Central PMCID: PMCPMC400619.
762 38. Mandecki W, Krajewska-Grynkiewicz K, Klopotowski T. A quantitative model for
763 nonrandom generalized transduction, applied to the phage P22-Salmonella typhimurium
764 system. Genetics. 1986;114(2):633-57. Epub 1986/10/01. PubMed PMID: 3021574;
765 PubMed Central PMCID: PMCPMC1202961.
766 39. Ebel-Tsipis J, Botstein D, Fox MS. Generalized transduction by phage P22 in
767 Salmonella typhimurium. I. Molecular origin of transducing DNA. J Mol Biol.
768 1972;71(2):433-48. Epub 1972/11/14. doi: 10.1016/0022-2836(72)90361-0. PubMed
769 PMID: 4564486.
770 40. Chiang YN, Penades JR, Chen J. Genetic transduction by phages and
771 chromosomal islands: The new and noncanonical. PLoS Pathog. 2019;15(8):e1007878.
772 Epub 20190808. doi: 10.1371/journal.ppat.1007878. PubMed PMID: 31393945; PubMed
773 Central PMCID: PMCPMC6687093.
774 41. Eggers CH, Gray CM, Preisig AM, Glenn DM, Pereira J, Ayers RW, et al. Phage-
775 mediated horizontal gene transfer of both prophage and heterologous DNA by varphiBB-
776 1, a bacteriophage of Borrelia burgdorferi. Pathog Dis. 2016;74(9). Epub 2016/11/05. doi:
777 10.1093/femspd/ftw107. PubMed PMID: 27811049.
778 42. Eggers CH. Identification and characterization of a bacteriophage of Borrelia
779 burgdorferi Graduate Student Theses, Dissertations, & Professional Papers 10590. 2000.
780 43. Rumnieks J, Fuzik T, Tars K. Structure of the Borrelia bacteriophage phiBB1
781 procapsid. J Mol Biol. 2023:168323. Epub 20231020. doi: 10.1016/j.jmb.2023.168323.
782 PubMed PMID: 37866476.
783 44. Eggers CH, Casjens S, Hayes SF, Garon CF, Damman CJ, Oliver DB, et al.
784 Bacteriophages of spirochetes. J Mol Microbiol Biotechnol. 2000;2(4):365-73. Epub
785 2000/11/15. PubMed PMID: 11075907.
786 45. Neubert U, Schaller M, Januschke E, Stolz W, Schmieger H. Bacteriophages
787 induced by ciprofloxacin in a Borrelia burgdorferi skin isolate. Zentralbl Bakteriol.
788 1993;279(3):307-15. doi: 10.1016/s0934-8840(11)80363-4. PubMed PMID: 8219501.
789 46. Gillis M, De Ley J, De Cleene M. The determination of molecular weight of bacterial
790 genome DNA from renaturation rates. Eur J Biochem. 1970;12(1):143-53. doi:
791 10.1111/j.1432-1033.1970.tb00831.x. PubMed PMID: 4984994.
792 47. Wood DE, Salzberg SL. Kraken: ultrafast metagenomic sequence classification
793 using exact alignments. Genome Biol. 2014;15(3):R46. Epub 20140303. doi: 10.1186/gb-
794 2014-15-3-r46. PubMed PMID: 24580807; PubMed Central PMCID: PMCPMC4053813.
795 48. Schutzer SE, Fraser-Liggett CM, Casjens SR, Qiu WG, Dunn JJ, Mongodin EF, et
796 al. Whole-genome sequences of thirteen isolates of Borrelia burgdorferi. J Bacteriol.
797 2011;193(4):1018-20. Epub 20101008. doi: 10.1128/JB.01158-10. PubMed PMID:
798 20935092; PubMed Central PMCID: PMCPMC3028687.
799 49. Casjens SR, Gilcrease EB. Determining DNA packaging strategy by analysis of
800 the termini of the chromosomes in tailed-bacteriophage virions. Methods Mol Biol.
801 2009;502:91-111. doi: 10.1007/978-1-60327-565-1_7. PubMed PMID: 19082553;
802 PubMed Central PMCID: PMCPMC3082370.
803 50. Garneau JR, Depardieu F, Fortier LC, Bikard D, Monot M. PhageTerm: a tool for
804 fast and accurate determination of phage termini and packaging mechanism using next-
805 generation sequencing data. Sci Rep. 2017;7(1):8292. Epub 20170815. doi:
806 10.1038/s41598-017-07910-5. PubMed PMID: 28811656; PubMed Central PMCID:
807 PMCPMC5557969.
808 51. Takacs CN, Kloos ZA, Scott M, Rosa PA, Jacobs-Wagner C. Fluorescent Proteins,
809 Promoters, and Selectable Markers for Applications in the Lyme Disease Spirochete

810 Borrelia burgdorferi. Appl Environ Microbiol. 2018;84(24). Epub 2018/10/14. doi:
811 10.1128/AEM.01824-18. PubMed PMID: 30315081; PubMed Central PMCID:
812 PMCPMC6275353.
813 52. Bailey TL, Boden M, Buske FA, Frith M, Grant CE, Clementi L, et al. MEME SUITE:
814 tools for motif discovery and searching. Nucleic Acids Res. 2009;37(Web Server
815 issue):W202-8. Epub 20090520. doi: 10.1093/nar/gkp335. PubMed PMID: 19458158;
816 PubMed Central PMCID: PMCPMC2703892.
817 53. Casjens S. Evolution of the linear DNA replicons of the Borrelia spirochetes. Curr
818 Opin Microbiol. 1999;2(5):529-34. doi: 10.1016/s1369-5274(99)00012-0. PubMed PMID:
819 10508719.
820 54. Tourand Y, Bankhead T, Wilson SL, Putteet-Driver AD, Barbour AG, Byram R, et
821 al. Differential telomere processing by Borrelia telomere resolvases in vitro but not in vivo.
822 J Bacteriol. 2006;188(21):7378-86. Epub 20060825. doi: 10.1128/JB.00760-06. PubMed
823 PMID: 16936037; PubMed Central PMCID: PMCPMC1636258.
824 55. Tourand Y, Kobryn K, Chaconas G. Sequence-specific recognition but position-
825 dependent cleavage of two distinct telomeres by the Borrelia burgdorferi telomere
826 resolvase, ResT. Mol Microbiol. 2003;48(4):901-11. doi: 10.1046/j.1365-
827 2958.2003.03485.x. PubMed PMID: 12753185.
828 56. Kobryn K, Chaconas G. Hairpin Telomere Resolvases. Microbiol Spectr.
829 2014;2(6). doi: 10.1128/microbiolspec.MDNA3-0023-2014. PubMed PMID: 26104454.
830 57. Huang WM, Robertson M, Aron J, Casjens S. Telomere exchange between linear
831 replicons of Borrelia burgdorferi. J Bacteriol. 2004;186(13):4134-41. doi:
832 10.1128/JB.186.13.4134-4141.2004. PubMed PMID: 15205414; PubMed Central
833 PMCID: PMCPMC421586.
834 58. Chaconas G, Stewart PE, Tilly K, Bono JL, Rosa P. Telomere resolution in the
835 Lyme disease spirochete. Embo J. 2001;20(12):3229-37. doi:
836 10.1093/emboj/20.12.3229. PubMed PMID: 11406599; PubMed Central PMCID:
837 PMCPMC150187.
838 59. Casjens S, Murphy M, DeLange M, Sampson L, van Vugt R, Huang WM.
839 Telomeres of the linear chromosomes of Lyme disease spirochaetes: nucleotide
840 sequence and possible exchange with linear plasmid telomeres. Mol Microbiol.
841 1997;26(3):581-96. doi: 10.1046/j.1365-2958.1997.6051963.x. PubMed PMID: 9402027.
842 60. Tourand Y, Deneke J, Moriarty TJ, Chaconas G. Characterization and in vitro
843 reaction properties of 19 unique hairpin telomeres from the linear plasmids of the lyme
844 disease spirochete. J Biol Chem. 2009;284(11):7264-72. Epub 20090102. doi:
845 10.1074/jbc.M808918200. PubMed PMID: 19122193; PubMed Central PMCID:
846 PMCPMC2652300.
847 61. Wilske B, Preac-Mursic V, Jauris S, Hofmann A, Pradel I, Soutschek E, et al.
848 Immunological and molecular polymorphisms of OspC, an immunodominant major outer
849 surface protein of Borrelia burgdorferi. Infect Immun. 1993;61(5):2182-91. doi:
850 10.1128/iai.61.5.2182-2191.1993. PubMed PMID: 8478108; PubMed Central PMCID:
851 PMCPMC280819.
852 62. Probert WS, Crawford M, Cadiz RB, LeFebvre RB. Immunization with outer
853 surface protein (Osp) A, but not OspC, provides cross-protection of mice challenged with
854 North American isolates of Borrelia burgdorferi. J Infect Dis. 1997;175(2):400-5. doi:
855 10.1093/infdis/175.2.400. PubMed PMID: 9203661.
856 63. Barthold SW. Specificity of infection-induced immunity among Borrelia burgdorferi
857 sensu lato species. Infect Immun. 1999;67(1):36-42. doi: 10.1128/IAI.67.1.36-42.1999.
858 PubMed PMID: 9864193; PubMed Central PMCID: PMCPMC96274.

859 64. Brisson D, Vandermause MF, Meece JK, Reed KD, Dykhuizen DE. Evolution of
860 northeastern and midwestern Borrelia burgdorferi, United States. Emerg Infect Dis.
861 2010;16(6):911-7. doi: 10.3201/eid1606.090329. PubMed PMID: 20507740; PubMed
862 Central PMCID: PMCPMC3086229.
863 65. Nadelman RB, Hanincova K, Mukherjee P, Liveris D, Nowakowski J, McKenna D,
864 et al. Differentiation of reinfection from relapse in recurrent Lyme disease. N Engl J Med.
865 2012;367(20):1883-90. doi: 10.1056/NEJMoa1114362. PubMed PMID: 23150958;
866 PubMed Central PMCID: PMCPMC3526003.
867 66. Bhatia B, Hillman C, Carracoi V, Cheff BN, Tilly K, Rosa PA. Infection history of
868 the blood-meal host dictates pathogenic potential of the Lyme disease spirochete within
869 the feeding tick vector. PLoS Pathog. 2018;14(4):e1006959. Epub 20180405. doi:
870 10.1371/journal.ppat.1006959. PubMed PMID: 29621350; PubMed Central PMCID:
871 PMCPMC5886588.
872 67. Kurtti TJ, Munderloh UG, Hughes CA, Engstrom SM, Johnson RC. Resistance to
873 tick-borne spirochete challenge induced by Borrelia burgdorferi strains that differ in
874 expression of outer surface proteins. Infect Immun. 1996;64(10):4148-53. doi:
875 10.1128/iai.64.10.4148-4153.1996. PubMed PMID: 8926082; PubMed Central PMCID:
876 PMCPMC174350.
877 68. Piesman J, Dolan MC, Happ CM, Luft BJ, Rooney SE, Mather TN, et al. Duration
878 of immunity to reinfection with tick-transmitted Borrelia burgdorferi in naturally infected
879 mice. Infect Immun. 1997;65(10):4043-7. doi: 10.1128/iai.65.10.4043-4047.1997.
880 PubMed PMID: 9317005; PubMed Central PMCID: PMCPMC175581.
881 69. Hofmeister EK, Glass GE, Childs JE, Persing DH. Population dynamics of a
882 naturally occurring heterogeneous mixture of Borrelia burgdorferi clones. Infect Immun.
883 1999;67(11):5709-16. doi: 10.1128/IAI.67.11.5709-5716.1999. PubMed PMID:
884 10531219; PubMed Central PMCID: PMCPMC96945.
885 70. Shang ES, Wu XY, Lovett MA, Miller JN, Blanco DR. Homologous and
886 heterologous Borrelia burgdorferi challenge of infection-derived immune rabbits using
887 host-adapted organisms. Infect Immun. 2001;69(1):593-8. doi: 10.1128/IAI.69.1.593-
888 598.2001. PubMed PMID: 11119560; PubMed Central PMCID: PMCPMC97926.
889 71. Derdakova M, Dudioak V, Brei B, Brownstein JS, Schwartz I, Fish D. Interaction
890 and transmission of two Borrelia burgdorferi sensu stricto strains in a tick-rodent
891 maintenance system. Appl Environ Microbiol. 2004;70(11):6783-8. doi:
892 10.1128/AEM.70.11.6783-6788.2004. PubMed PMID: 15528545; PubMed Central
893 PMCID: PMCPMC525125.
894 72. Khatchikian CE, Nadelman RB, Nowakowski J, Schwartz I, Wormser GP, Brisson
895 D. Evidence for strain-specific immunity in patients treated for early lyme disease. Infect
896 Immun. 2014;82(4):1408-13. Epub 20140113. doi: 10.1128/IAI.01451-13. PubMed PMID:
897 24421042; PubMed Central PMCID: PMCPMC3993397.
898 73. Dykhuizen DE, Polin DS, Dunn JJ, Wilske B, Preac-Mursic V, Dattwyler RJ, et al.
899 Borrelia burgdorferi is clonal: implications for taxonomy and vaccine development. Proc
900 Natl Acad Sci U S A. 1993;90(21):10163-7. doi: 10.1073/pnas.90.21.10163. PubMed
901 PMID: 8234271; PubMed Central PMCID: PMCPMC47734.
902 74. Stevenson B, Barthold SW. Expression and sequence of outer surface protein C
903 among North American isolates of Borrelia burgdorferi. FEMS Microbiol Lett.
904 1994;124(3):367-72. doi: 10.1111/j.1574-6968.1994.tb07310.x. PubMed PMID:
905 7851744.
906 75. Jauris-Heipke S, Liegl G, Preac-Mursic V, Rossler D, Schwab E, Soutschek E, et
907 al. Molecular analysis of genes encoding outer surface protein C (OspC) of Borrelia
908 burgdorferi sensu lato: relationship to ospA genotype and evidence of lateral gene

909 exchange of ospC. J Clin Microbiol. 1995;33(7):1860-6. doi: 10.1128/jcm.33.7.1860-
910 1866.1995. PubMed PMID: 7665660; PubMed Central PMCID: PMCPMC228286.
911 76. Livey I, Gibbs CP, Schuster R, Dorner F. Evidence for lateral transfer and
912 recombination in OspC variation in Lyme disease Borrelia. Mol Microbiol. 1995;18(2):257-
913 69. doi: 10.1111/j.1365-2958.1995.mmi_18020257.x. PubMed PMID: 8709845.
914 77. Will G, Jauris-Heipke S, Schwab E, Busch U, Rossler D, Soutschek E, et al.
915 Sequence analysis of ospA genes shows homogeneity within Borrelia burgdorferi sensu
916 stricto and Borrelia afzelii strains but reveals major subgroups within the Borrelia garinii
917 species. Med Microbiol Immunol. 1995;184(2):73-80. doi: 10.1007/BF00221390. PubMed
918 PMID: 7500914.
919 78. Hefty PS, Brooks CS, Jett AM, White GL, Wikel SK, Kennedy RC, et al. OspE-
920 related, OspF-related, and Elp lipoproteins are immunogenic in baboons experimentally
921 infected with Borrelia burgdorferi and in human lyme disease patients. J Clin Microbiol.
922 2002;40(11):4256-65. Epub 2002/11/01. PubMed PMID: 12409407; PubMed Central
923 PMCID: PMCPMC139709.
924 79. Tilly K, Bestor A, Rosa PA. Functional Equivalence of OspA and OspB, but Not
925 OspC, in Tick Colonization by Borrelia burgdorferi. Infect Immun. 2016;84(5):1565-73.
926 Epub 20160422. doi: 10.1128/IAI.00063-16. PubMed PMID: 26953324; PubMed Central
927 PMCID: PMCPMC4862709.
928 80. Battisti JM, Bono JL, Rosa PA, Schrumpf ME, Schwan TG, Policastro PF. Outer
929 surface protein A protects Lyme disease spirochetes from acquired host immunity in the
930 tick vector. Infect Immun. 2008;76(11):5228-37. Epub 20080908. doi: 10.1128/IAI.00410-
931 08. PubMed PMID: 18779341; PubMed Central PMCID: PMCPMC2573341.
932 81. Yang XF, Pal U, Alani SM, Fikrig E, Norgard MV. Essential role for OspA/B in the
933 life cycle of the Lyme disease spirochete. J Exp Med. 2004;199(5):641-8. Epub
934 20040223. doi: 10.1084/jem.20031960. PubMed PMID: 14981112; PubMed Central
935 PMCID: PMCPMC2213294.
936 82. Wang IN, Dykhuizen DE, Qiu W, Dunn JJ, Bosler EM, Luft BJ. Genetic diversity of
937 ospC in a local population of Borrelia burgdorferi sensu stricto. Genetics. 1999;151(1):15-
938 30. doi: 10.1093/genetics/151.1.15. PubMed PMID: 9872945; PubMed Central PMCID:
939 PMCPMC1460459.
940 83. Lemieux JE, Huang W, Hill N, Cerar T, Freimark L, Hernandez S, et al. Whole
941 genome sequencing of human Borrelia burgdorferi isolates reveals linked blocks of
942 accessory genome elements located on plasmids and associated with human
943 dissemination. PLoS Pathog. 2023;19(8):e1011243. Epub 20230831. doi:
944 10.1371/journal.ppat.1011243. PubMed PMID: 37651316; PubMed Central PMCID:
945 PMCPMC10470944.
946 84. Streisinger G, Emrich J, Stahl MM. Chromosome structure in phage t4, iii. Terminal
947 redundancy and length determination. Proc Natl Acad Sci U S A. 1967;57(2):292-5. doi:
948 10.1073/pnas.57.2.292. PubMed PMID: 16591467; PubMed Central PMCID:
949 PMCPMC335503.
950 85. Beaulaurier J, Luo E, Eppley JM, Uyl PD, Dai X, Burger A, et al. Assembly-free
951 single-molecule sequencing recovers complete virus genomes from natural microbial
952 communities. Genome Res. 2020;30(3):437-46. Epub 2020/02/23. doi:
953 10.1101/gr.251686.119. PubMed PMID: 32075851; PubMed Central PMCID:
954 PMCPMC7111524.
955 86. Skare JT, Champion CI, Mirzabekov TA, Shang ES, Blanco DR, Erdjument-
956 Bromage H, et al. Porin activity of the native and recombinant outer membrane protein
957 Oms28 of Borrelia burgdorferi. J Bacteriol. 1996;178(16):4909-18. doi:

10.1128/jb.178.16.4909-4918.1996. PubMed PMID: 8759855; PubMed Central PMCID: PMCPMC178274.

87. Kasumba IN, Tilly K, Lin T, Norris SJ, Rosa PA. Strict Conservation yet Non-Essential Nature of Plasmid Gene bba40 in the Lyme Disease Spirochete Borrelia burgdorferi. Microbiol Spectr. 2023;11(3):e0047723. Epub 20230403. doi: 10.1128/spectrum.00477-23. PubMed PMID: 37010416; PubMed Central PMCID: PMCPMC10269632.

88. Barbour AG, Garon CF. Linear plasmids of the bacterium Borrelia burgdorferi have covalently closed ends. Science. 1987;237(4813):409-11. doi: 10.1126/science.3603026. PubMed PMID: 3603026.

89. Hinnebusch J, Tilly K. Linear plasmids and chromosomes in bacteria. Mol Microbiol. 1993;10(5):917-22. doi: 10.1111/j.1365-2958.1993.tb00963.x. PubMed PMID: 7934868.

90. Marconi RT, Casjens S, Munderloh UG, Samuels DS. Analysis of linear plasmid dimers in Borrelia burgdorferi sensu lato isolates: implications concerning the potential mechanism of linear plasmid replication. J Bacteriol. 1996;178(11):3357-61. doi: 10.1128/jb.178.11.3357-3361.1996. PubMed PMID: 8655522; PubMed Central PMCID: PMCPMC178094.

91. Pahl A, Kuhlbrandt U, Brune K, Rollinghoff M, Gessner A. Quantitative detection of Borrelia burgdorferi by real-time PCR. J Clin Microbiol. 1999;37(6):1958-63. doi: 10.1128/JCM.37.6.1958-1963.1999. PubMed PMID: 10325354; PubMed Central PMCID: PMCPMC84995.

92. Lanfear R, Schalamun M, Kainer D, Wang W, Schwessinger B. MinIONQC: fast and simple quality control for MinION sequencing data. Bioinformatics. 2019;35(3):523-5. doi: 10.1093/bioinformatics/bty654. PubMed PMID: 30052755; PubMed Central PMCID: PMCPMC6361240.

93. Wick RR, Judd LM, Gorrie CL, Holt KE. Completing bacterial genome assemblies with multiplex MinION sequencing. Microb Genom. 2017;3(10):e000132. Epub 20170914. doi: 10.1099/mgen.0.000132. PubMed PMID: 29177090; PubMed Central PMCID: PMCPMC5695209.

94. Li H. Minimap2: pairwise alignment for nucleotide sequences. Bioinformatics. 2018;34(18):3094-100. doi: 10.1093/bioinformatics/bty191.

95. Danecek P, Bonfield JK, Liddle J, Marshall J, Ohan V, Pollard MO, et al. Twelve years of SAMtools and BCFtools. GigaScience. 2021;10(2). doi: 10.1093/gigascience/giab008.

96. Shen W, Le S, Li Y, Hu F. SeqKit: A Cross-Platform and Ultrafast Toolkit for FASTA/Q File Manipulation. PLOS ONE. 2016;11(10):e0163962. doi: 10.1371/journal.pone.0163962.

97. Wick RR, Judd LM, Cerdeira LT, Hawkey J, Méric G, Vezina B, et al. Trycycler: consensus long-read assemblies for bacterial genomes. Genome Biology. 2021;22(1). doi: 10.1186/s13059-021-02483-z.

98. Kolmogorov M, Yuan J, Lin Y, Pevzner PA. Assembly of long, error-prone reads using repeat graphs. Nature Biotechnology. 2019;37(5):540-6. doi: 10.1038/s41587-019-0072-8.

99. Vaser R, Šikić M. Time- and memory-efficient genome assembly with Raven. Nature Computational Science. 2021;1(5):332-6. doi: 10.1038/s43588-021-00073-4.

100. Wick RR, Holt KE. Benchmarking of long-read assemblers for prokaryote whole genome sequencing. F1000Research. 2021;8:2138. doi: 10.12688/f1000research.21782.4.

101. Zuker M. Mfold web server for nucleic acid folding and hybridization prediction. Nucleic Acids Research. 2003;31(13):3406-15. doi: 10.1093/nar/gkg595.
102. Samuels DS. Electrotransformation of the spirochete Borrelia burgdorferi. Methods Mol Biol. 1995;47:253-9. doi: 10.1385/0-89603-310-4:253. PubMed PMID: 7550741; PubMed Central PMCID: PMCPMC5815860.
103. Bunikis I, Kutschan-Bunikis S, Bonde M, Bergstrom S. Multiplex PCR as a tool for validating plasmid content of Borrelia burgdorferi. J Microbiol Methods. 2011;86(2):243-7. Epub 20110512. doi: 10.1016/j.mimet.2011.05.004. PubMed PMID: 21605603.
104. Fu L, Niu B, Zhu Z, Wu S, Li W. CD-HIT: accelerated for clustering the next-generation sequencing data. Bioinformatics. 2012;28(23):3150-2. Epub 20121011. doi: 10.1093/bioinformatics/bts565. PubMed PMID: 23060610; PubMed Central PMCID: PMCPMC3516142.
105. Grant CE, Bailey TL, Noble WS. FIMO: scanning for occurrences of a given motif. Bioinformatics. 2011;27(7):1017-8. Epub 20110216. doi: 10.1093/bioinformatics/btr064. PubMed PMID: 21330290; PubMed Central PMCID: PMCPMC3065696.
106. Crooks GE, Hon G, Chandonia JM, Brenner SE. WebLogo: a sequence logo generator. Genome Res. 2004;14(6):1188-90. Epub 2004/06/03. doi: 10.1101/gr.849004. PubMed PMID: 15173120; PubMed Central PMCID: PMCPMC419797.
107. Katoh K, Standley DM. MAFFT multiple sequence alignment software version 7: improvements in performance and usability. Mol Biol Evol. 2013;30(4):772-80. Epub 20130116. doi: 10.1093/molbev/mst010. PubMed PMID: 23329690; PubMed Central PMCID: PMCPMC3603318.
108. Nguyen LT, Schmidt HA, von Haeseler A, Minh BQ. IQ-TREE: a fast and effective stochastic algorithm for estimating maximum-likelihood phylogenies. Mol Biol Evol. 2015;32(1):268-74. Epub 20141103. doi: 10.1093/molbev/msu300. PubMed PMID: 25371430; PubMed Central PMCID: PMCPMC4271533.
109. Minh BQ, Nguyen MA, von Haeseler A. Ultrafast approximation for phylogenetic bootstrap. Mol Biol Evol. 2013;30(5):1188-95. Epub 20130215. doi: 10.1093/molbev/mst024. PubMed PMID: 23418397; PubMed Central PMCID: PMCPMC3670741.
110. Bianchini G, Sánchez-Baracaldo P. TreeViewer - Cross-platform software to draw phylogenetic trees. 2023. doi: https://doi.org/10.5281/zenodo.7768343.